Biogeosciences, 10, 2169–2191, 2013
www.biogeosciences.net/10/2169/2013/
doi:10.5194/bg-10-2169-2013

Biogeosciences Open Access

Global ocean storage of anthropogenic carbon

S. Khatiwala[1], T. Tanhua[2], S. Mikaloff Fletcher[3], M. Gerber[4], S. C. Doney[5], H. D. Graven[6], N. Gruber[6], G. A. McKinley[7], A. Murata[8], A. F. Ríos[9], and C. L. Sabine[10]

[1]Lamont-Doherty Earth Observatory of Columbia University, Palisades, NY, USA
[2]Helmholtz Centre for Ocean Research Kiel, Marine Biogeochemistry, Kiel, Germany
[3]National Institute of Water and Atmospheric Research, 301 Evans Bay Pde., Hataitai, Wellington, New Zealand
[4]Climate and Environmental Physics, Physics Institute, University of Bern, Switzerland; and Oeschger Centre for Climate Change Research, University of Bern, Switzerland
[5]Woods Hole Oceanographic Institution, MA, USA
[6]Institute of Biogeochemistry and Pollutant Dynamics, ETH Zurich, Switzerland
[7]Atmospheric and Ocean Sciences, University of Wisconsin – Madison, WI, USA
[8]Research Institute of Global Change, Japan Agency for Marine-Earth Science and Technology, Yokosuka, Japan
[9]Instituto de Investigaciones Marinas, IIM-CSIC, C/Eduardo Cabello 6, 36208 Vigo, Spain
[10]NOAA Pacific Marine Environmental Laboratory, Seattle, WA, USA

Correspondence to: S. Khatiwala (spk@ldeo.columbia.edu)

Received: 15 June 2012 – Published in Biogeosciences Discuss.: 23 July 2012
Revised: 27 January 2013 – Accepted: 25 February 2013 – Published: 2 April 2013

Abstract. The global ocean is a significant sink for anthropogenic carbon (C_{ant}), absorbing roughly a third of human CO_2 emitted over the industrial period. Robust estimates of the magnitude and variability of the storage and distribution of C_{ant} in the ocean are therefore important for understanding the human impact on climate. In this synthesis we review observational and model-based estimates of the storage and transport of C_{ant} in the ocean. We pay particular attention to the uncertainties and potential biases inherent in different inference schemes. On a global scale, three data-based estimates of the distribution and inventory of C_{ant} are now available. While the inventories are found to agree within their uncertainty, there are considerable differences in the spatial distribution. We also present a review of the progress made in the application of inverse and data assimilation techniques which combine ocean interior estimates of C_{ant} with numerical ocean circulation models. Such methods are especially useful for estimating the air–sea flux and interior transport of C_{ant}, quantities that are otherwise difficult to observe directly. However, the results are found to be highly dependent on modeled circulation, with the spread due to different ocean models at least as large as that from the different observational methods used to estimate C_{ant}. Our review also highlights the importance of repeat measurements of hydrographic and biogeochemical parameters to estimate the storage of C_{ant} on decadal timescales in the presence of the variability in circulation that is neglected by other approaches. Data-based C_{ant} estimates provide important constraints on forward ocean models, which exhibit both broad similarities and regional errors relative to the observational fields. A compilation of inventories of C_{ant} gives us a "best" estimate of the global ocean inventory of anthropogenic carbon in 2010 of 155 ± 31 PgC (± 20 % uncertainty). This estimate includes a broad range of values, suggesting that a combination of approaches is necessary in order to achieve a robust quantification of the ocean sink of anthropogenic CO_2.

1 Introduction

The release of fossil fuel CO_2 to the atmosphere by human activity has been implicated as the predominant cause of global climate change (Denman et al., 2007). The ocean plays a crucial role in mitigating the effects of this perturbation to the climate system, having to date sequestered roughly a third of cumulative anthropogenic CO_2 emissions from the atmosphere. There are indications, however, that the oceanic carbon sink may have changed during the past few decades

(Wetzel et al., 2005; Le Quéré et al., 2007; Lovenduski et al., 2007; Le Quéré et al., 2010; Pérez et al., 2010), although significant uncertainties remain (e.g., McKinley et al., 2011). Quantifying the oceanic carbon inventory and its variability is therefore important for understanding the global carbon cycle and how it might change over time.

Estimating the storage of anthropogenic CO_2 (C_{ant}) in the ocean is a difficult task for a variety of reasons. First, C_{ant} is not a directly measurable quantity; it has to be inferred using indirect means. Second, the C_{ant} signal in the ocean is only a small perturbation (of order of a few percent at the most) on the natural or preindustrial background distribution of carbon. A further complication is that carbon in the ocean participates in complex in situ biogeochemistry. Lastly, the C_{ant} distribution in the ocean is rather heterogeneous. As a consequence, unlike the atmosphere, which is relatively well mixed and where observations (both direct and from ice cores) extend back many thousands of years, the ocean is much more challenging in this regard.

Historically, estimates of C_{ant} have been based on indirect techniques, such as the so-called "back-calculation" methods, whose basic principles go back to the late 1970s (Brewer, 1978; Chen and Millero, 1979). These methods attempt to separate the small anthropogenic perturbation from the large background distribution of carbon by correcting the measured total dissolved inorganic carbon (DIC) concentration for changes due to biological activity and by removing an estimate of the preindustrial preformed DIC concentration. These early applications were met by strong scepticism (Broecker et al., 1985), and it required significant improvements in methodology, notably the development of the ΔC^* approach (Gruber et al., 1996) (see Sabine and Tanhua (2010) for a comprehensive review), and the availability of a high quality and consistent global biogeochemical data set (e.g., Key et al., 2004), before this approach found general acceptance. These advances led to the first observation-based global estimates of the distribution of C_{ant} in the ocean (Sabine et al., 2004).

A more recent development is the use of a transit time distribution (TTD) (Hall et al., 2002; Waugh et al., 2004), or more generally a Green's function (GF) (Holzer and Hall, 2000; Khatiwala et al., 2001, 2009), to describe the transport of anthropogenic CO_2 from the surface into the interior. Tracer observations are used to constrain the TTD (Waugh et al., 2006) or Green's function (Khatiwala et al., 2009). Unlike the back-calculation scheme, this approach has the advantage of accounting for mixing between waters of different ages, and has been most recently applied to reconstruct the time-varying distribution of C_{ant} over the industrial era (Khatiwala et al., 2009).

Observational estimates of C_{ant} have also been combined with ocean general circulation models (OGCMs) in an "inverse" scheme to obtain air–sea fluxes and interior ocean transport of C_{ant} consistent with the data-based C_{ant} estimate (e.g., Gloor et al., 2003; Mikaloff Fletcher et al., 2006; Gerber et al., 2009; Gerber and Joos, 2010). The data-based estimates also provide important constraints for evaluating C_{ant} fields from forward integrations of OGCMs (e.g., Sarmiento et al., 1992; Orr et al., 2001, 2005; Gruber et al., 2009; Wang et al., 2012), the same OGCMs that are used commonly to study future climate impacts on ocean carbon storage (e.g., Fung et al., 2005; Roy et al., 2011).

Here, we review estimates of the interior ocean storage, air–sea flux, and interior transport of C_{ant} based on a variety of methods. We define C_{ant} as the excess amount of DIC that is present in the water column due to the increasing atmospheric concentration of CO_2 and the resulting higher flux of CO_2 to the oceans compared to the preindustrial ocean. Our focus will be on global ocean estimates based on measurements, including inverse approaches, and comparisons to forward simulations. We provide both an extensive discussion of the various methods used to estimate C_{ant} as well as their biases and uncertainties.

2 Observation-based estimates of C_{ant}

2.1 Methods

The back-calculation and the TTD/GF-based methods differ fundamentally in the way they approach the estimation of the distribution of C_{ant} in the ocean: The back-calculation method, such as the ΔC^* method, starts with ocean observations of DIC and aims to tease out the anthropogenic perturbation, while the TTD/GF methods start with a mathematical description of how the ocean's circulation connects surface boundary conditions with interior ocean concentrations of tracers and them aims to "calibrate" these processes through tracer observations.

In any back-calculation approach, C_{ant} is estimated in a two-step approach. First, the changes in the measured DIC that incurred since a water parcel (or a set of mixtures of water parcels) left the surface due to the remineralization of organic matter or the dissolution of biogenic calcium carbonate are removed on the basis of concurrently measured O_2, nutrients, alkalinity and the assumption of fixed stoichiometric ratios. In the second step, the preindustrial preformed DIC is estimated and removed as well, with the residual interpreted as the anthropogenic CO_2 component. While the earlier implementation made relatively simple assumptions to estimate the preindustrial preformed DIC, the ΔC^* method suggested splitting this estimation problem into an equilibrium part, which can be estimated accurately on the basis of the well-known carbonate chemistry and an air–sea disequilibrium part (Gruber et al., 1996). Furthermore, it was suggested to estimate this disequilibrium through a combination of analyses of very old waters assumed to be void of C_{ant} and the use of age tracers (cf. Gruber (1998)). Gruber et al. (1996) and all subsequent applications of the ΔC^* method assumed that the disequilibrium remained unchanged through the

anthropogenic transient, although it is fundamentally possible to include a time-varying disequilibrium in the estimation procedure as well (Matsumoto and Gruber, 2005). The ΔC^* method was applied by Sabine et al. (2004) to the Global Ocean Data Analysis Project (GLODAP) data set (Key et al., 2004) to arrive at a near-global estimate of the distribution and inventory of C_{ant} in the ocean.

A method conceptually similar to the ΔC^* approach, known as TrOCA, was introduced by Touratier and Goyet (2004) with a more recent formulation provided by Touratier et al. (2007). This method is based on a conservative tracer (TrOCA) defined from oxygen, DIC and total alkalinity (A_T), similarly to classical conservative tracers such as "NO" or "PO" (Broecker, 1974; Ríos et al., 1989). The C_{ant} concentration is estimated by subtracting from TrOCA a zero-C_{ant} reference (TrOCA°) defined from the "natural" concentrations of oxygen, DIC and A_T. The equation for the reference term TrOCA° is a non-linear function of temperature and A_T. The TrOCA approach is quite straightforward because it uses one simple equation for the global ocean. When used in the Atlantic Ocean, it gives C_{ant} inventories comparable to those obtained by other approaches (Vázquez-Rodríguez et al., 2009b). Nonetheless, the use of a universal equation may produce overestimates of 50 % in the global C_{ant} inventory relative to other inference schemes (Yool et al., 2010).

The C°_{IPSL} method (Lo Monaco et al., 2005b) is based on the original C° method described by Brewer (1978) and Chen and Millero (1979), and was further updated by Körtzinger et al. (1998). This scheme allows for air–sea oxygen disequilibrium in the surface ocean; it uses different relationships of A°_T and DIC° for southern and northern Atlantic waters based on observations collected in their source regions (Körtzinger et al., 1998), and a mixing model based on optimum multi-parameter (OMP) analysis to constrain their relative contributions. The preindustrial C_{ant} reference is calculated from North Atlantic Deep Water (NADW) detected in the South Atlantic, where C_{ant} concentrations are below detection limits. This zero-C_{ant} baseline reference corresponds to the increase in DIC° in the source region since the preindustrial era, and although it is a time-dependent parameter it is applied as a constant. Moreover, this term should have a temperature dependence (Friis, 2006) leading to higher C_{ant} estimates than those given by the TTD and ϕC°_T methods (Vázquez-Rodríguez et al., 2009b).

The ϕC°_T method (Vázquez-Rodríguez et al., 2009a,b) shares similar fundamentals with the ΔC^* back-calculation method. In this approach, the subsurface layer (100–200 m) is taken as a reference for characterizing water mass properties, specifically A°_T and air–sea CO_2 disequilibrium (ΔC_{dis}), at the time of their formation. These parameters (expressed in terms of conservative tracers) are obtained from subsurface data and applied directly to calculate C_{ant} in waters above the 5 °C isotherm, and via an OMP analysis for waters below. This procedure particularly improves estimates in cold deep waters that are subject to strong and complex mixing processes between northern and southern source waters. One important feature of the ϕC°_T method is that it does not rely on CFC data. In addition, the method attempts to approximate the temporal and spatial variability of ΔC_{dis} in the Atlantic Ocean in terms of C_{ant} and ΔC_{dis} itself (Vázquez-Rodríguez et al., 2012). The ϕC°_T method was originally formulated for the Atlantic Ocean but, using new parameterizations for A°_T and ΔC_{dis}, has been recently applied to the Pacific and Indian oceans (Pardo et al., 2011).

A more recently developed approach, proposed by Hall et al. (2002), is to exploit the smallness of the anthropogenic perturbation in the ocean by treating C_{ant} as a conservative tracer, that is, a tracer that is not influenced by biological processes in the ocean. The transport of any such tracer in the ocean can be described as a continuous, joint distribution of the time and surface location at which a water parcel was last exposed to the atmosphere. This distribution, known as the "boundary propagator" (Holzer and Hall, 2000), is a type of Green's function, i.e., a solution to the advection–diffusion equation for the ocean with an impulse boundary condition at the surface of the ocean. The Green function, $\mathcal{G}$, is an intrinsic property of the ocean circulation and not specific to any particular tracer. It can thus be convolved with the time history of that tracer in the surface mixed layer of the ocean to compute the interior concentration of that tracer at any given point in space and time. The anthropogenic CO_2 concentration at location $\mathbf{x}$ and time t is then given by

$$C_{ant}(\mathbf{x}, t) = \int_{surface} d^2x' \int_{-\infty}^{t} dt' C^s_{ant}(\mathbf{x}', t')\mathcal{G}(\mathbf{x}, t|\mathbf{x}', t'), \qquad (1)$$

where C^s_{ant} is the surface history of C_{ant}. This approach recognizes the fact that in the presence of mixing there is no single ventilation time, and it avoids the need for complex and uncertain biological corrections (although it is implicitly assumed that biology is in a steady state), as in the ΔC^* method. To apply this formalism, Waugh et al. (2006) made a number of simplifications. First, they assumed that a single surface source region dominates the C_{ant} at each interior location, i.e., there is negligible mixing of water masses with different source regions. The resulting Green function, then, only depends on the time elapsed since a water parcel was last in contact with the surface and is known as the transit time distribution (TTD; Holzer and Hall, 2000). Second, they assumed that the ocean's TTD can be approximated by the solution to the 1-D advection–diffusion equation (Hall et al., 2002). This solution, known as the "inverse Gaussian" (Seshadri, 1999), is parameterized by two variables (a mean and width). Assuming that the ratio of mean age to width is known (and taken to be "1"), they estimated the mean using CFC-12 observations from the GLODAP data set. Lastly, they assumed constant air–sea disequilibrium to estimate the unknown surface boundary condition for C_{ant}. With these simplifications, Waugh et al. (2006) arrived at a global estimate of C_{ant} in the ocean.

Most recently, Khatiwala et al. (2009) have developed an inverse technique to apply the full Green function formalism. Specifically, they (1) applied a maximum entropy deconvolution technique (Tarantola, 2005) to constrain the Green function with multiple steady and transient tracers and thus account for the mixing of waters of both different ages and different end-member types and (2) allowed the air–sea disequilibrium to evolve in space and time. To reduce the indeterminacy, the surface integral in Eq. (1) is discretized into a finite number of surface patches and a boundary propagator computed with respect to each patch. In order to estimate the C_{ant} surface history, they impose the condition that the rate of change of inventory of C_{ant} is equal to the instantaneous air–sea flux of C_{ant}. The latter flux is proportional to the change in surface disequilibrium of CO_2 relative to the preindustrial disequilibrium, which, in turn, is assumed to be proportional to the anthropogenic CO_2 perturbation in the atmosphere (see also Matsumoto and Gruber, 2005). Khatiwala et al. (2009) applied this method to gridded fields of six different tracers from the GLODAP data set (CFC-11, CFC-12, natural ^{14}C, salinity, temperature, and PO_4^* (Broecker et al., 1998)) to arrive at the first data-based estimate of the time-evolving, three-dimensional history of anthropogenic CO_2 in the ocean over the industrial period. In the following, we term their approach the "Green function (GF) method" to distinguish it from the simpler TTD approach (Waugh et al., 2006).

For comparison, we also include in the analysis model-estimated C_{ant} inventories and distributions from forward integrations of two global OGCMs. (We restrict ourselves to models participating in the Regional Carbon Cycle Assessment and Processes (RECCAP) study and for which the requisite data are available.) The first set of forward ocean model simulations were created with the low-resolution ocean physics component of the Community Climate System Model (CCSM-3) (Yeager et al., 2006). All of the CCSM-3 simulations are at a resolution of 0.9–1.9°latitude by 3.6°longitude with 25 vertical levels, and incorporate a dynamic upper-ocean ecosystem model (phytoplankton/zooplankton/nutrient) coupled with a full-depth carbon cycle biogeochemistry module treating both dissolved inorganic carbon and alkalinity prognostically (Doney et al., 2009b,a). For each reported model case, a pair of model simulations with identical physical circulation was conducted, a preindustrial control with fixed atmospheric CO_2 and an anthropogenic transient simulation with prescribed historical atmospheric CO_2; C_{ant} is calculated from the difference of the anthropogenic minus preindustrial simulations.

The CCSM variants, CCSM-ETH (Graven et al., 2012) and CCSM-WHOI (Doney et al., 2009a), differ in the preindustrial spin-up procedures and applied atmospheric physical forcing. Repeat annual physical forcing cycles ("normal-year forcing") (Large and Yeager, 2004) were used during the model preindustrial spin-up and atmospheric CO_2 transient from the early 19th century through the middle of the 20th century for all of the CCSM runs, and in the CCSM-ETH-cnst case normal-year forcing was used also for the remainder of the 20th century and early 21st century. The CCSM-ETH-var and CCSM-WHOI cases utilized time-varying atmospheric forcing after the mid-20th century based on NCEP reanalysis (CCSM-WHOI) and the Common Ocean-ice Reference Experiments (CORE) forcing (CCSM-ETH-var), which is derived from the NCEP reanalysis but includes a variety of corrections (Large and Yeager, 2004). Gas exchange in all the CCSM cases is calculated from the NCEP (or CORE) winds and a quadratic wind speed parameterization similar to Wanninkhof (1992). In the CCSM-ETH simulations, the parameter in the wind speed relationship was scaled down from the originally proposed value in order to arrive at a global mean gas transfer velocity of $15\,cm\,hr^{-1}$. This adjustment was based on recent reanalyses of the global radiocarbon constraints on the rate of the air–sea transfer, which suggested a ∼30 % reduction in this parameter (Sweeney et al., 2007; Graven et al., 2012). In the CCSM-ETH-var-k19 case, the original parameter was used, yielding a global mean gas transfer velocity of $19\,cm\,hr^{-1}$). The CCSM-WHOI simulations were carried out with the original parameter, yielding, with the NCEP winds, a global mean gas transfer velocity of $21\,cm\,hr^{-1}$.

A final forward ocean model simulation case, ECCO (Graven et al., 2012), was generated with the physical ocean state estimate from the Estimating the Circulation and Climate of the Ocean (ECCO) consortium (Stammer et al., 2004). The ECCO ocean state estimate was achieved by adjusting the air–sea fluxes of heat, momentum and freshwater in the MIT OGCM (Marshall et al., 1997) through data assimilation (Wunsch and Heimbach, 2007). This procedure results in a dynamically consistent estimate of ocean circulation and hydrography over the assimilation period. The model has a horizontal resolution of 1° with 23 vertical levels. In the ECCO case, dissolved inorganic carbon was simulated according to the "abiotic" formulation of the Ocean Carbon-Cycle Model Intercomparison Project 2 (OCMIP-2) (Orr et al., 1999). Local air–sea gas exchange velocities were calculated from the Wanninkhof (1992) parameterization using the CORE normal-year winds (i.e., different winds from those used to drive the circulation), with a coefficient scaled to result in a global mean gas exchange velocity of $15\,cm\,hr^{-1}$. Carbon simulations were performed using the transport matrix method, an "offline" method for simulation of biogeochemical tracers (Khatiwala, 2007, 2008). Monthly mean transport matrices, representing a climatology over the 1992–2004 assimilation period, were extracted from the model and used to perform the tracer simulations. Comparing ECCO with CCSM demonstrates the impact of differing physical circulation on CO_2 uptake and storage, as well as the impact of data assimilation. These two models are representative of the range of C_{ant} inventories in current ocean models (Graven et al., 2012).

It is important to note that the GF estimate presented here is not completely independent of ECCO. The maximum

entropy inverse method used by the former requires a prior estimate of the Green function. In previous published studies using this method, the prior was computed by fitting an inverse Gaussian form to CFC-12 data, assuming a mean/width ratio of "1". In the version here, a TTD was simulated using the annually averaged ECCO circulation field with an impulse boundary condition at the surface of the ocean (no spatial variation). This simulated TTD was then spatially averaged over $20^\circ \times 20^\circ$ boxes and a mean/width ratio computed for each box. This ratio rather than unity was then used when fitting the inverse Gaussian form to compute the prior. (At any location, the same prior is used for all the boundary propagators for the various surface patches.) The reasoning behind this procedure was to arrive at an improved prior (as a mean/width ratio of 1 is not always justified), yet one not too dependent on a model. Thus, information from the ECCO model about where water at any given location comes from, or the corresponding timescales, was not computed or used, and this procedure leads to results that are practically similar to those in which a ratio of 1 was used.

2.2 Results from global estimates

Near-global estimates based on the three approaches described above (ΔC^*, TTD, and GF) are available for the reference year 1994. In addition, the GF estimate is a time-evolving reconstruction between 1765 and 2008. For the reference year 1994, the near-global ocean inventories (without marginal seas) are (1) 106 ± 17 PgC based on the ΔC^* method (Sabine et al., 2004), (2) 94–121 PgC based on the TTD method (Waugh et al., 2006), and (3) 114 ± 22 PgC using the Green function approach (Khatiwala et al., 2009) (see Table 1 for a summary). Note that for the ΔC^* estimate, unphysical negative concentrations were set to zero before computing the inventory (a roughly 10 % upward correction), and a 20 % downward correction was applied by Waugh et al. (2006) to the TTD-based global inventory to account for a positive bias arising from assuming a constant air–sea disequilibrium (see below). This correction was derived by applying the TTD method to tracer fields simulated in an ocean biogeochemical model. For the present study, the GF estimate has been extended in time through 2010, and it is 150 ± 26 PgC for the year 2010 (Fig. 1).

The above estimates are all based on the GLODAP data set, which does not cover coastal regions and several marginal seas, most notably the Arctic, the Caribbean, and the Mediterranean seas. Recent work, however, shows that, relative to their area, these excluded regions store proportionately more C_{ant} compared with the global ocean and thus contribute significant C_{ant} to their respective adjacent major basins. Estimates for several marginal basins, including the Arctic (Tanhua et al., 2009), the Nordic seas (Olsen et al., 2010), the Mediterranean Sea (Schneider et al., 2010), and the East Sea (Sea of Japan) (Park et al., 2006), are now available (see Fig. 1). With the exception of the Park et al. (2006) estimate, which applied a modified version of the ΔC^* technique, these are based on the TTD method. The marginal seas and coastal areas for which the inventory of C_{ant} has been quantified add up to roughly 8.6 ± 0.6 PgC for reference year 2010 (Lee et al., 2011), i.e., approximately 6 % of the global ocean C_{ant} storage (the open ocean and marginal seas summing to 160 ± 26 PgC). However, as there are additional marginal seas and coastal areas for which the C_{ant} inventory has yet to be quantified, this is a lower bound of their contribution to the global C_{ant} inventory.

To put the above estimates into context, the total cumulative emissions from fossil fuel burning and cement production from 1750 through 2009 are around 350 PgC (Andres et al., 2012). An additional 180 ± 50 PgC has been emitted due to land use changes (Houghton et al., 1999). The ocean inventory therefore represents ~ 45 % of fossil fuel CO_2 emissions over the industrial period, consistent with the earlier work of Sabine et al. (2004) who found that the ocean inventory accounted for nearly half of the fossil fuel CO_2 emitted since the preindustrial era. Assuming total anthropogenic emissions since 1750 of 530 PgC, the relative uptake ratio for the ocean is ~ 30 %. We note that these values are based on the total accumulation of CO_2 in the ocean since the preindustrial era. However, both the emission and ocean uptake rates vary significantly over time. Thus, measured as a fraction of current annual fossil fuel and total emission rates of $8.5\,\mathrm{PgC\,y^{-1}}$ and $10\,\mathrm{PgC\,y^{-1}}$, respectively, the contemporary ocean sink of $\sim 2.5\,\mathrm{PgC\,y^{-1}}$ (Khatiwala et al., 2009) accounts for 1/3 and 1/4 of fossil fuel and total emissions, respectively.

While the above global estimates agree to within their uncertainty, there are significant differences in the spatial distribution of C_{ant}, particularly at high latitudes. Figures 2, 3, and 4 show the column inventory (also known as "specific inventory"), zonal mean sections for each ocean basin, and basin-averaged vertical profiles, respectively, of C_{ant} in 1994 for the three data-based estimates. Also shown are corresponding fields from the various forward ocean model simulations. All estimates display a similar pattern of strong accumulation of C_{ant} in the North Atlantic, and high concentrations ranging around $45–55\,\mu\mathrm{mol\,kg^{-1}}$ in the surface layer. C_{ant} decays rapidly with depth until ~ 1000 m, and then remains more or less constant.

As noted by Wang et al. (2012) in a detailed comparison of various data-based estimates, there is generally good agreement in the upper ocean, but pronounced differences can be found in intermediate and deep waters. The ΔC^* method generally gives the lowest values, including spurious, negative concentrations in deep waters (Sabine et al., 2004; Waugh et al., 2006). These likely resulted from uncertainties associated with the separation of the end-members and the estimation of their disequilibria. Since these negative concentrations are unphysical, they were set to zero when computing inventories. The TTD method typically produces the highest values. These are believed to be due to the

Table 1. Summary of C_{ant} inventories in 1994 estimated by different observational methods and simulated in numerical models. For the model-based estimates, numbers in brackets represent inventories for the region covered by the GLODAP database.

Method	C_{ant} inventory [PgC]	Reference
Green's function	114 ± 22	Khatiwala et al. (2009)
ΔC^*	106 ± 17	Sabine et al. (2004)
TTD	94–121	Waugh et al. (2006)
ECCO	124 (116)	Graven et al. (2012)
CCSM-ETH-var	95 (85)	Graven et al. (2012)
CCSM-ETH-cnst	94 (83)	Graven et al. (2012)
CCSM-ETH-var-k19	97 (86)	Graven et al. (2012)
CCSM-WHOI	89 (80)	Doney et al. (2009a)

Table 2. Summary of C_{ant} inventories in 2010 (mid-year or annual mean) estimated by different observational methods and simulated in numerical models. Inventories for both the region covered by the GLODAP database (second column) and (for estimates involving models) the original grid (third column) are shown. In some instances the estimate has been scaled from the original year of reference to 2010 using the transient steady state (TSS) approach (see text), as indicated in the fourth column.

Method	C_{ant} inventory [PgC] (GLODAP region)	C_{ant} inventory [PgC]	TSS Scaling
Data-based estimates			
Green's function	150 ± 26	–	None
ΔC^*	138 ± 21	–	From 1994
TTD	122–157	–	From 1994
ENKF-ΔC^*	132	145	From 2008.5
ENKF-TTD	138	151	From 2008.5
OIP	149	158	From 2005
Model-based estimates			
ECCO	152	162	None
CCSM-ETH-var	110	124	From 2007.5
CCSM-ETH-cnst	107	121	From 2007.5
CCSM-ETH-var-k19	112	126	From 2007.5
CCSM-WHOI	106	119	None

assumption of constant disequilibrium, which predicts higher concentrations in the surface layer than would be the case if the disequilibrium were allowed to evolve (and increase) in time (see below). These high values are then propagated by the TTD into the interior. The GF method does not make this assumption; it also allows for mixing between different water masses. GF-based estimates are consequently intermediate between the ΔC^* and TTD estimates. Integrating over various ocean basins, Wang et al. (2012) concluded that the best agreement was found in the Indian Ocean, with estimates ranging from 13 to 14 PgC. Estimates of C_{ant} in the Pacific Ocean also agree well, ranging from 29 to 35 PgC. The largest differences were found in the Southern Ocean (see Fig. 2), ranging from 30 PgC (ΔC^* method) to 49 PgC (TTD method). The GF method was intermediate with 36 PgC.

Relative to the data-based estimates, the CCSM simulations tend to underestimate the global C_{ant} inventory (89–97 PgC) while the ECCO global inventory (124 PgC) falls within the reported data-based range (Fig. 2). Note that, for comparison with the data-based estimates, Fig. 2 indicates both the total inventory simulated by the models as well as the inventory in the regions covered by the GLODAP observations. Applying the GLODAP mask generally reduces model inventories by $\sim$10 PgC, further increasing the negative bias of the CCSM simulations but bringing the ECCO value closer to the observations. Graven et al. (2012) argue on the basis of their comparison of the simulated changes in the ^{14}C distribution with the observed ones that the CCSM-ETH and ECCO simulations provide useful constraints on the likely range of oceanic uptake of C_{ant}. Strengthening the rate of gas exchange in the CCSM-ETH model (CCSM-ETH-k19) yields only a small increase of 2 PgC in the global C_{ant} inventory relative to the CCSM-ETH-var case, consistent with earlier model results showing that ocean transport is the dominant limiting factor in anthropogenic carbon uptake (Sarmiento et al., 1992). Similarly, the use of time-varying versus repeat annual atmospheric forcing has only a minor (1 PgC) impact on the global C_{ant} inventory, although there are regional differences, notably in the Atlantic basin (Fig. 5) (see also Levine et al. (2011) and Wang et al. (2012)).

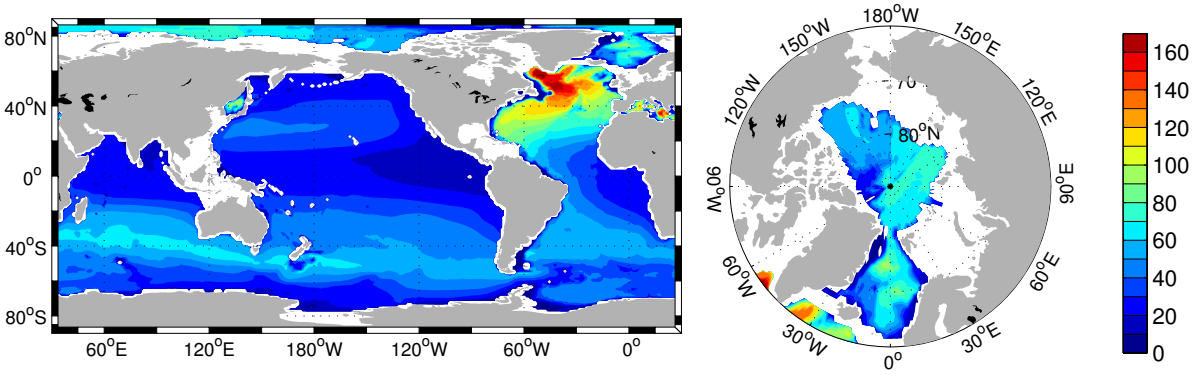

Fig. 1. Compilation of 2010 column inventories (mol m^{-2}) of anthropogenic CO_2: the global ocean excluding the marginal seas, 150±26 PgC (Khatiwala et al., 2009); Arctic Ocean, 2.7–3.5 PgC (Tanhua et al., 2009); the Nordic seas, 1.0–1.6 PgC (Olsen et al., 2010); the Mediterranean Sea, 1.6–2.5 PgC (Schneider et al., 2010); and the East Sea (Sea of Japan), 0.40 ± 0.06 PgC (Park et al., 2006).

The simulated spatial patterns of the column inventories are broadly similar to those from data-based estimates with elevated inventories in the North Atlantic and Southern oceans (Fig. 2), but there are substantial differences at regional scales and in the simulated vertical distributions (see Figs. 3 and 4). CCSM-simulated surface C_{ant} values are lower than all of the data-based estimates for the Southern Ocean, which Long et al. (submitted) argue arises in a later variant of the CCSM from negative biases in simulated surface alkalinity – and hence the buffer factor – that lead to the model surface ocean saturating too quickly with respect to a perturbation in atmospheric CO_2. This may be due to possible errors in the CCSM prognostic $CaCO_3$ cycle in this region, such as the dissolution of sinking $CaCO_3$ occurring at too great a depth. Errors in surface C_{ant} will eventually propagate into the interior for waters ventilated from that region. On the other hand, errors in circulation tend to lead to errors primarily in the deep ocean C_{ant}, whereas the surface ocean values are much less affected. In general, however, both factors are likely to play a role in causing the mismatch. CCSM surface values are in better agreement with the GF estimates in the other basins, although there is a range in surface values even within the data-based estimates.

The CCSM simulations tend to underestimate C_{ant} storage at mid-latitudes in the mid- to lower thermocline, similar to the vertical biases exhibited in the suite of OCMIP-2 models even after they had been optimized to fit the ΔC^*-based C_{ant} estimates (Mikaloff Fletcher et al., 2006). The vertical penetration of C_{ant} in the CCSM simulations is also noticeably weaker than the data-based estimates in intermediate and deep waters in the North Atlantic and intermediate waters of the South Atlantic, which likely reflects too-shallow and too-weak formation of North Atlantic Deep Water, a common problem in z-coordinate OGCMs (Doney et al., 2004). A low C_{ant} bias is also found in the thermocline and intermediate depths in the Southern Ocean, contributing to the low column inventory relative to the data-based methods. The Southern Ocean C_{ant} bias is associated with a similar bias in model chlorofluorocarbon uptake and appears to reflect too-weak physical ventilation of mode and intermediate waters (Long et al., 2012). The CCSM model exhibits small, unphysical negative C_{ant} values in the deep Indo-Pacific basins due to tracer advection artifacts.

By contrast, the ECCO simulation does a better job capturing the vertical distribution of C_{ant} compared to the data-based estimates (Figs. 3 and 4) and is in fact very similar to the GF estimate. The primary, if small, difference is that ECCO values tend to be slightly higher in the upper ocean (particularly in the North Atlantic) and lower in the deep ocean (especially in the Pacific). The state estimation procedure appears to improve aspects of the ocean circulation in the lower thermocline and intermediate depths where the unconstrained CCSM has problems in replicating C_{ant}. The specific mechanisms and whether insights from ECCO can be used to improve the physical forcing and model parameterizations for unconstrained models remain a topic for further research.

2.3 Uncertainties

There are a large number of sources of error and uncertainty in data-based estimates of anthropogenic CO_2. These range from sparse sampling and random uncertainty to systematic biases due to the assumptions made by each method. We discuss these in turn below.

Random sources of uncertainty: There are several published estimates of the uncertainty in the calculation of C_{ant} based on different methods (see Table A1 in the appendix). Gruber et al. (1996) assessed the uncertainty in the C_{ant} concentration estimated via a back-calculation method to be $\pm 9\,\mu mol\,kg^{-1}$ for the Atlantic Ocean. They obtained this value by propagating errors analytically over the precision limits of the various measurements required for solving their C_{ant} estimation equations. Applying their approach to

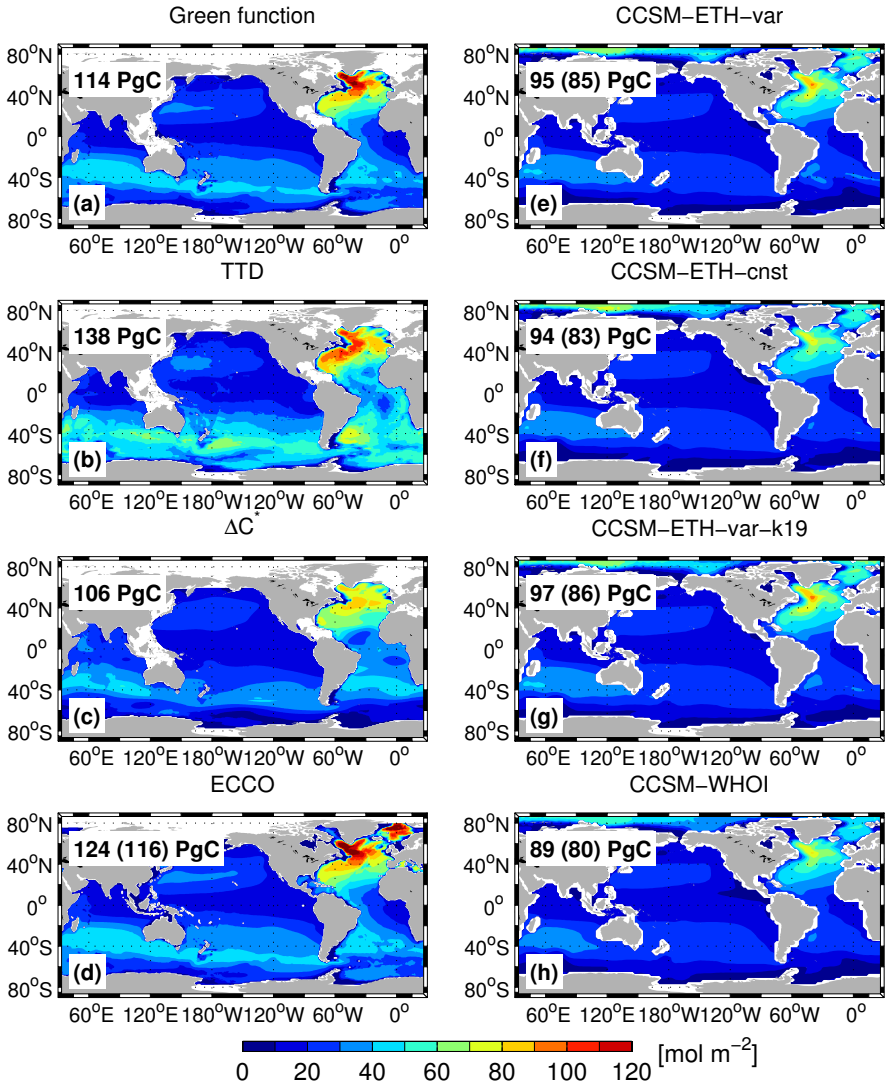

Fig. 2. Column inventory of C_{ant} in mol m^{-2} in 1994 based on various data-based methods (panels **a**–**c**) and forward model simulations (panels **d**–**h**). Also indicated on each panel (top left corner) is the C_{ant} inventory in PgC and, for the forward models, the inventory (numbers in brackets) for the region covered by the GLODAP tracer data set on which the observational estimates are based. No downward correction (see text) was applied to the global inventory based on the TTD method.

other methods has yielded an uncertainty between ±5 and ±8 µmol kg^{-1} (e.g., Lee et al., 2003; Waugh et al., 2006; Vázquez-Rodríguez et al., 2009b). However, since several terms and properties involved in the calculation act in opposite directions, perturbation propagation techniques tend to produce lower estimates of uncertainty (Lo Monaco et al., 2005a). In deep and homogenous waters with very low C_{ant} levels, Ríos et al. (2003) found absolute uncertainties as low as 3 µmol kg^{-1}; i.e., the uncertainty is of the same order of magnitude as the C_{ant} concentration. The uncertainty of C_{ant} estimates using the TTD method is spatially variable and dependent on, for instance, the transient of the tracer used for determining the TTD and the analytical uncertainty of the tracer measurements (Tanhua et al., 2008). In the Green function approach, a maximum entropy deconvolution technique is used to estimate the ocean's transport Green's function from tracer data. Since only a limited number of observational constraints are available, the problem is highly underdetermined, leading to errors in the estimated Green function. This so-called "entropic uncertainty" (Holzer et al., 2010) can lead to large errors in pointwise estimates of C_{ant} concentration, although spatial integration to compute inventories significantly reduces the error (Holzer et al., 2010). There are also errors arising from the sparse spatial and temporal sampling of the various tracers used in the inversion. Khatiwala et al. (2009) applied a Monte Carlo procedure in

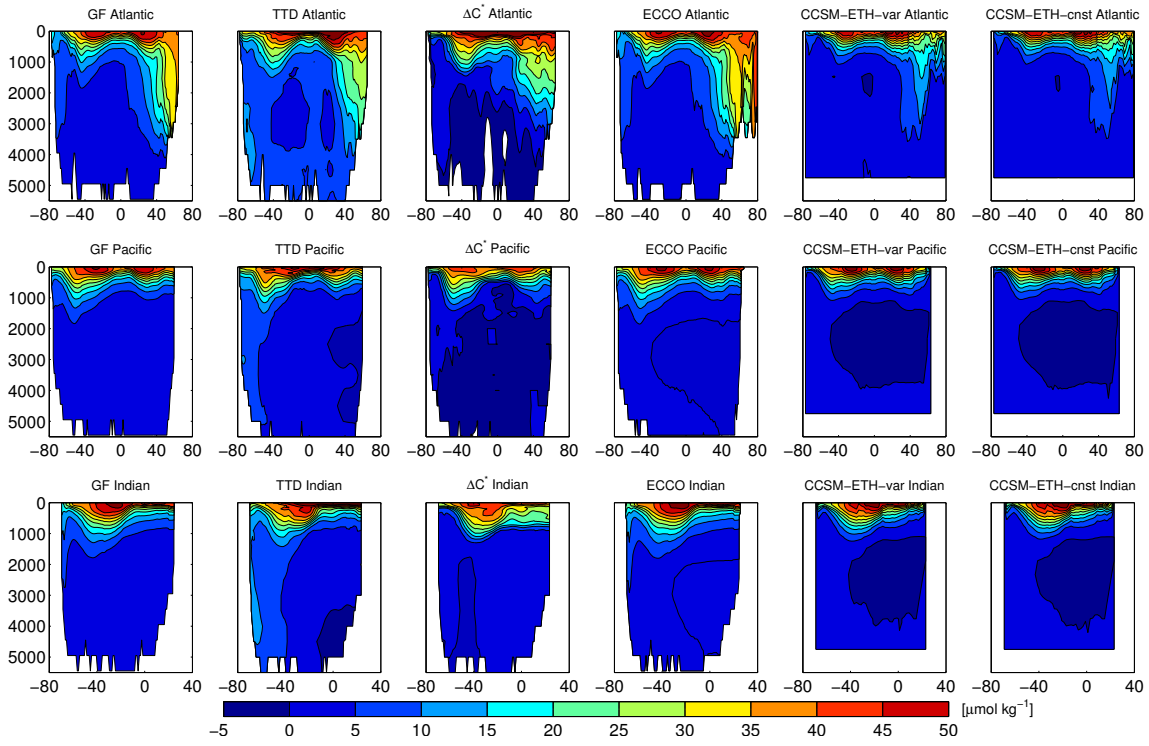

Fig. 3. Zonal mean sections of C_{ant} in 1994 estimated by three data-based methods and three forward ocean model simulations. Top to bottom: Atlantic, Pacific, and Indian oceans; left to right: Green's function, TTD, ΔC^*, ECCO, CCSM-ETH-var, and CCSM-ETH-cnst.

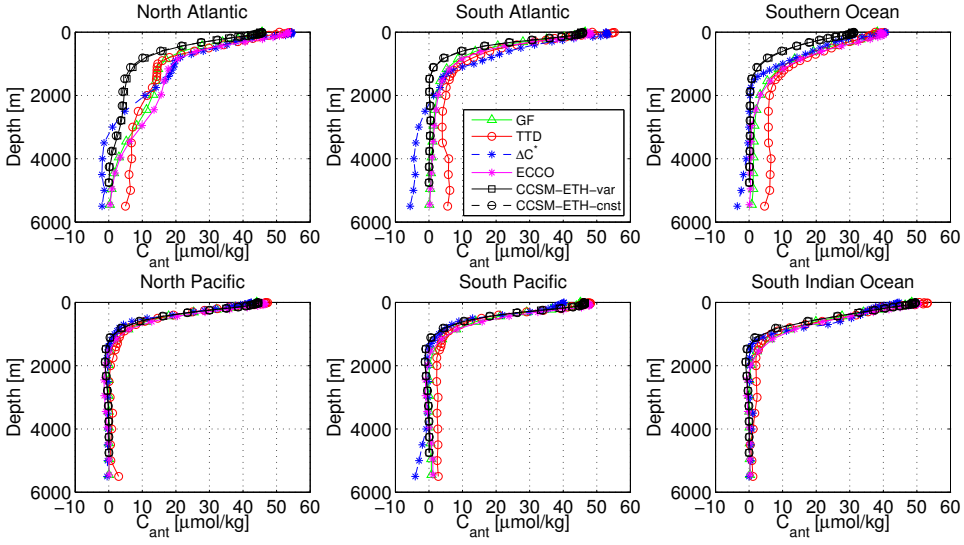

Fig. 4. Basin-averaged vertical profiles of C_{ant} in 1994 estimated by three data-based methods and three forward ocean model simulations. The Southern Ocean is defined as the region south of 35° S. No corrections have been applied to either the TTD or ΔC^* data (see text).

which the calculation of the Green function and C_{ant} was repeated by randomly sampling the various parameters used in the inversion from a uniform distribution centered about its observed value and width equal to the reported uncertainty. This approach combined with the entropic uncertainty leads to a (spatially variable) uncertainty between ± 2 and $\pm 8\,\mu mol\,kg^{-1}$.

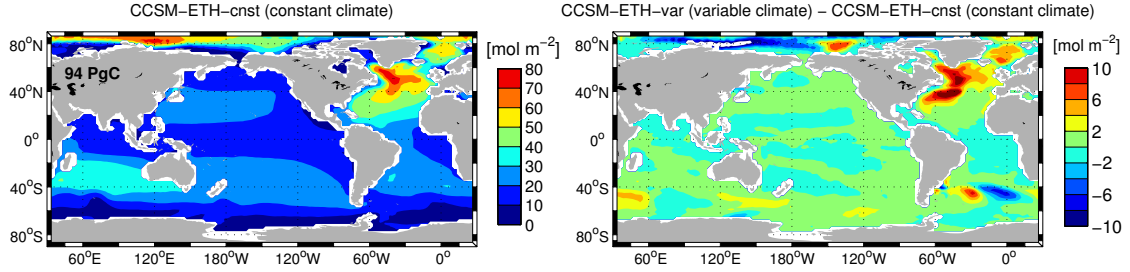

Fig. 5. Comparison of anthropogenic CO_2 simulated in the CCSM-ETH model under constant climate (CCSM-ETH-cnst) and with time-varying climate (CCSM-ETH-var). Left: Column inventory of anthropogenic CO_2 in 1994 simulated in the constant-climate simulation. Right: Difference in column inventory in 1994 between variable-climate and constant-climate simulations. (Note the different scales.) The total inventory in the constant-climate case was 94 PgC, while that in the variable simulation was 95 PgC.

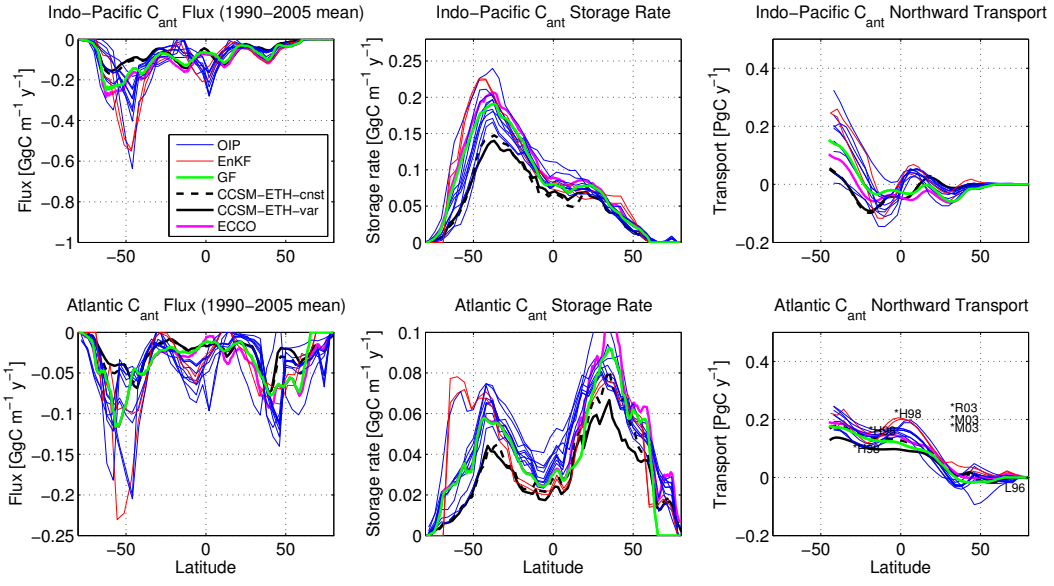

Fig. 6. The air–sea flux (left), interior storage (middle), and transport (right) of anthropogenic CO_2 for the Indo-Pacific (top) and Atlantic (bottom) basins estimated using the Green function method, ocean inversions, and forward ocean models. In keeping with the RECCAP convention, negative flux values represent a flux out from the atmosphere into the ocean. Blue lines represent the ten OGCMs used by Mikaloff Fletcher et al. (2006); red lines represent two of the various anthropogenic CO_2 determination methods (ΔC^* and TTD) used by Gerber et al. (2009) in their EnKF calculation; green lines are estimates based on the Green function approach; broken and solid black lines represent the CCSM-ETH-var and CCSM-ETH-cnst simulations, respectively; and pink lines represent the ECCO simulation. Positive (negative) transports indicate northward (southward) transport. The ocean inversion estimates the integrated flux and storage of anthropogenic carbon since 1765, but we have scaled these values to 2005 using the atmospheric CO_2 perturbation. Symbols in the bottom right panel represent transect-based transport estimates in the Atlantic from Holfort et al. (1998); Rosón et al. (2003); Macdonald et al. (2003); Lundberg and Haugan (1996).

Errors in individual C_{ant} estimates propagate into uncertainty in column and regional inventories. A perturbation procedure was recently applied (Álvarez et al., 2009; Vázquez-Rodríguez et al., 2009b) using the random uncertainties for each back-calculation technique to evaluate this error to be $\pm 2.0\,\mathrm{mol\,m^{-2}}$. In regions with high interannual variability, as in the North Atlantic subpolar gyre, Pérez et al. (2008) also considered the variability of the thickness in the water masses. Using this procedure, Vázquez-Rodríguez et al. (2009b) estimated the uncertainty in column inventories to be $\pm 1\,\mathrm{mol\,m^{-2}}$ when integrated down to 3000 m, assuming random propagation of a $5\,\mu\mathrm{mol\,kg^{-1}}$ standard error in the C_{ant} concentration (see Table A2 in the Appendix). However, the vertical interpolation error is highly dependent on the (vertical) sampling density, particularly in high density gradient parts of the water column.

Ultimately, the goal is often to produce an estimate of the C_{ant} inventory for an ocean basin or the global ocean. In addition to the errors discussed above, additional uncertainties associated with interpolation to produce a gridded data set are present. These are sensitive to the mapping technique used. For example, both the ΔC^* and TTD methods were applied to discrete bottle data from GLODAP and the resulting C_{ant} estimates subsequently gridded using an objective mapping procedure that also quantifies mapping errors (Key et al., 2004; Waugh et al., 2006). In contrast, the GF technique was directly applied to the objectively gridded tracer fields from GLODAP. The corresponding error field was then used in the Monte Carlo procedure described above. Thus, the GF uncertainty estimate only partly and implicitly accounts for mapping errors. In either case, mapping errors can be as large as 10–20 % of the inventory (Sabine et al., 2004; Waugh et al., 2006) (see Table A3 in the Appendix).

Biases due to assumptions: All the estimation techniques make assumptions that are difficult to test, but efforts using simulated data in ocean biogeochemical models have been made to evaluate the validity of specific assumptions and the ability of the various methods to accurately estimate C_{ant} (e.g., Matsumoto and Gruber, 2005). Common to all data-based methods is the assumption that ocean circulation and biogeochemistry have remained constant over the industrial period. Thus, both natural and anthropogenically induced variability in physical and biological processes are neglected. Wang et al. (2012) have recently used the CCSM-3 to investigate this assumption. They find that the difference in global inventory of C_{ant} over the period 1948–2003 between a constant-climate simulation and one in which surface forcing and ocean circulation are allowed to vary is less than 1 % of the total inventory (similar to results for CCSM-ETH in Fig. 2). Moreover, when changes in the natural carbon cycle are also accounted for, the difference is still less than 4 % of the total anthropogenic inventory. Thus, the error in global inventory due to neglecting the impact of changing climate on both the natural carbon system and the uptake of C_{ant} is currently much smaller than the intrinsic uncertainty of the various methods (typically 20 %; see above). (This, of course, may not hold in the future as the ocean responds to climate change (Goodkin et al., 2011).) Regionally, however, the errors can be quite significant (Fig. 5) and of the same order of magnitude as the uncertainty in data-based estimates (Table A2).

Other systematic sources of errors depend on the specific assumptions made by each technique. The ΔC^* method assumes constant Redfield ratios, a constant air–sea disequilibrium, and that ocean circulation is largely advective in nature, justifying the use of a single (typically CFC-based) ventilation age (although in some implementations (e.g., Lee et al., 2003) mixing between different water masses is taken into account when computing the air–sea disequilibrium term). The latter assumption, in particular, can lead to an overestimate in the upper water column, because tracer ages are biased young, but a negative bias in the deeper waters without detectable CFC concentrations (which are then assumed to be free of anthropogenic CO_2) (Hall et al., 2002, 2004; Waugh et al., 2004). In the subpolar North Atlantic, for example, this assumption leads to uptake being overestimated by 20–30 % (Waugh et al., 2004). The assumption of a constant disequilibrium also leads to a significant bias, as shown by Matsumoto and Gruber (2005) in their evaluation of the ΔC^* method. Although the usual application of the ΔC^* method leads to substantial compensatory effects, the method was found to generally overestimate anthropogenic CO_2 in the upper thermocline by about 10 % and to underestimate it in the deep ocean. Overall, they concluded that the global inventory based on the ΔC^* method was probably too large by 7 %.

The TTD approach also assumes constant disequilibrium, and, while it relaxes the assumption of no mixing, it only considers a single water mass and uptake source region, as well as a particular and simplified functional form for the TTD. To evaluate the TTD method, Waugh et al. (2006) applied it to the output of an ocean biogeochemical model. They found that inferred C_{ant} concentrations and column inventories in all regions except the Southern Ocean agreed within $1\,\mu mol\,kg^{-1}$ and 10 % with the "true" (simulated) values. In the Southern Ocean, however, differences of 2–$6\,\mu mol\,kg^{-1}$ were found, leading to a positive bias of 60 % in the regional inventory and 20 % in the global inventory. (The TTD method also overestimates C_{ant} by about $2.5\,\mu mol\,kg^{-1}$ in deep waters when the CFC-12 concentration is near the detection limit (Waugh et al., 2006); values less than $2.5\,\mu mol\,kg^{-1}$ are set to zero when computing inventories.)

Although the Green function approach does not assume a constant disequilibrium, it needs to make another simplifying assumption in order to derive the time-varying surface history of C_{ant}: that the change in surface disequilibrium is proportional to the change in the atmospheric CO_2 concentration. Khatiwala et al. (2009) justified this relationship on the basis of simulations in a carbon cycle model. In a detailed examination of this assumption in an ocean biogeochemical model, Wang et al. (2012) found that, while a linear relationship between changes in air–sea disequilibrium and changes in atmospheric CO_2 is a good approximation under constant climate, there are substantial errors on regional and interannual scales when variability in ocean circulation is allowed. These errors, which propagate into estimates of the surface C_{ant} boundary condition and hence interior concentrations, however, largely cancel out upon temporal and spatial averaging (as performed by Khatiwala et al. (2009) in their application of the Green function method).

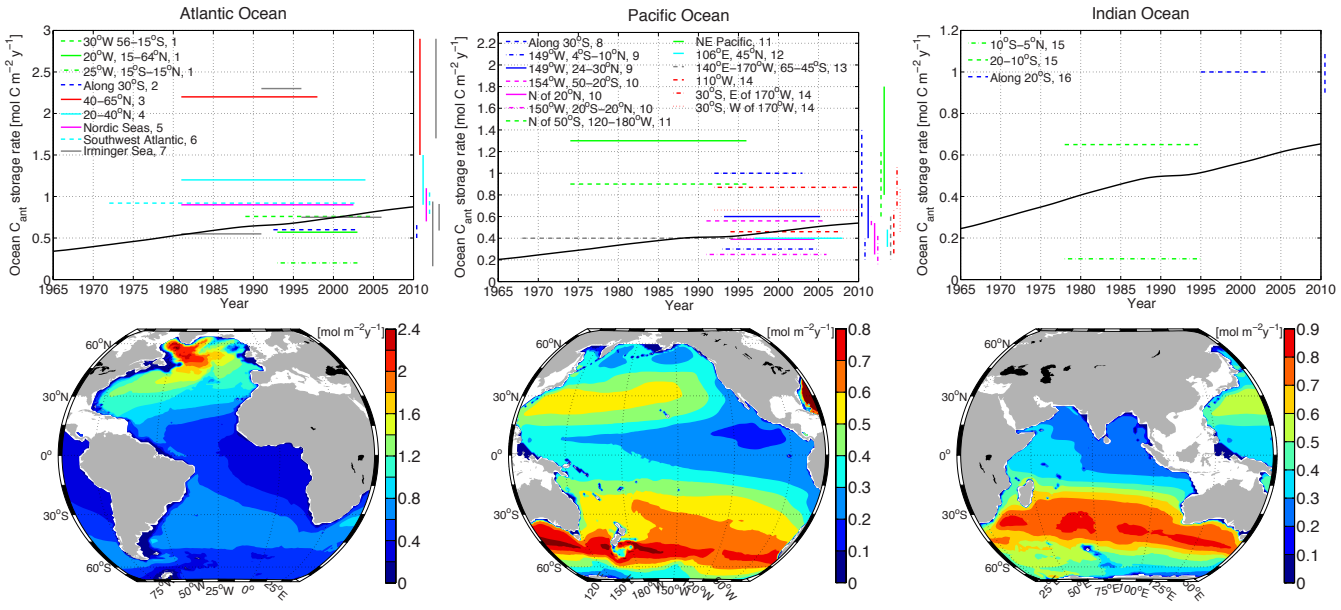

Fig. 7. Storage rates of anthropogenic carbon ([mol m^{-2} y^{-1}]) for the Atlantic (left), Pacific (center), and Indian oceans (right), based on repeat hydrography (top) and the GF inversion (bottom). Measurements for the Northern Hemisphere are drawn as solid lines, the tropics as dash-dotted lines, and dashed lines for the Southern Hemisphere; the color schemes refer to different studies. The solid black line in each panel is the time-varying basin mean storage rate estimated by the Green function approach (Khatiwala et al., 2009). Estimates of uncertainties are shown as vertical bars with matching colors. Maps on the bottom show the corresponding storage rate distribution from the GF inversion averaged over 1980–2005. Data sources are as indicated in the legends in the top row panels. (1) Wanninkhof et al. (2010), (2) Murata et al. (2008), (3) Friis et al. (2005), (4) Tanhua et al. (2007), (5) Olsen et al. (2006), (6) Ríos et al. (2012), (7) Pérez et al. (2008), (8) Murata et al. (2007), (9) Murata et al. (2009), (10) Sabine et al. (2008), (11) Peng et al. (2003), (12) Wakita et al. (2010), (13) Matear and McNeil (2003), (14) Waters et al. (2011), (15) Peng et al. (1998), and (16) Murata et al. (2010).

3 Ocean inversions and transport

3.1 The inverse approach

An important limitation of the data-based estimates discussed above is that these methods generally do not provide interior transport rates or surface air–sea fluxes of C_{ant} (although the GF method does simultaneously provide estimates of the average flux on a discrete set of surface patches). The availability of data assimilation techniques has, however, made it possible to combine global estimates of C_{ant} concentration with ocean circulation models to derive such information. Thus far, two techniques have been used to infer optimal air–sea fluxes of CO_2 from ocean interior C_{ant} data: a basis function approach and an ensemble Kalman filter (EnKF) technique.

The basis function approach is analogous to a method that has been widely used to estimate sources and sinks of atmospheric CO_2 based on atmospheric observations and atmospheric transport models (e.g., Enting and Mansbridge, 1989; Tans et al., 1990; Bousquet et al., 2000). This method has been adapted to estimate air–sea fluxes of heat (Gloor et al., 2001), oxygen (Gruber et al., 2001), and CO_2 (Gloor et al., 2003; Mikaloff Fletcher et al., 2006; Mikaloff Fletcher et al., 2007; Gruber et al., 2009) using ocean interior observations and OGCMs. This approach also shares many similarities with the GF method in that it aims to determine the connection between surface fluxes and interior concentrations, with the key difference being that the ocean inversion uses models to simulate the Green function, whereas the GF method uses transient and hydrographic observations to constrain it (no inorganic carbon parameters are used). The two approaches could therefore be described as "model-based GF" and "empirical GF", respectively.

In the ocean inversion scheme, the ocean is divided into discrete surface patches, and an OGCM is used to generate a basis function for each patch, which describes how an arbitrary flux into that region influences observations. The observed property, C_{ant}, is described as a linear combination of model-generated basis functions, A_i, each multiplied with a scaling factor, λ_i, plus an error, ϵ_i:

$$C_{ant} = \sum_{i=1,nreg} \lambda_i A_i + \epsilon_i. \quad (2)$$

The basis function for each region was generated by continuously injecting an arbitrary amount of a dye flux into the surface of the region in an OGCM. This dye flux is distributed spatially based on an air–sea flux climatology

$P_n(i, j, t)$ (Takahashi et al., 2002). In the case of the inversion of anthropogenic CO_2, the flux must also be scaled with time using an atmospheric scaling factor, $\phi(t)$, to account for changes in the atmospheric CO_2 concentration over the industrial period (Gloor et al., 2003; Mikaloff Fletcher et al., 2006). For region n the injected flux then reads

$$F_n(i, j, t) = \lambda_n P_n(i, j, t)\phi(t). \quad (3)$$

The EnKF technique applied by Gerber et al. (2009) used a similar regional air–sea flux pattern and temporal scaling to inject a dye tracer into the surface of an OGCM. However, in this case an ensemble of simulations integrated with a prescribed model circulation, each with a different set of air–sea CO_2 flux parameters, was run forward over the industrial period. This ensemble was then optimized in the framework of an EnKF (Evensen, 2003). After the optimization, the ensemble of simulations is reinitialized with the optimized set of parameters and is run again forward in time. This procedure is repeated until the optimized parameters converge. For details we refer to Gerber et al. (2009) and Gerber and Joos (2010).

3.2 Fluxes, transport, and storage of anthropogenic carbon in the interior ocean

The three-dimensional storage of anthropogenic CO_2 in the interior ocean can be calculated from the optimized air–sea flux estimates and the ocean model simulations used in the inversion. The transport of anthropogenic CO_2 can be subsequently calculated from the divergence of the regional fluxes estimated from the inversion and the corresponding storage. The basis function approach, as part of the Ocean Inversion Project (OIP), has been applied to the ΔC^*-based estimates using 10 different OGCMs. The EnKF scheme has been applied to C_{ant} estimates based on several different methods, including ΔC^* and TTD. In each case, the EnKF was used to estimate air–sea fluxes, using model transport from four different realizations of ocean circulation produced by varying physical model parameters such as the diapycnal diffusivity in the Bern OGCM (Gerber et al., 2009). Figure 6 shows the inversely estimated flux (top), storage (center), and transport (bottom), for both the basis function and EnKF approaches, using a range of different OGCMs and anthropogenic CO_2 reconstruction techniques. Displayed values for the basis function estimates have been scaled to 2005 based on the atmospheric CO_2 perturbation that was used to calculate the basis functions, assuming that the inventory and transports for each region increase proportionally with the perturbation to atmospheric CO_2. For comparison, we also show the GF-based estimate and forward ocean model results from CCSM-ETH and ECCO. Note that the transports for these cases were computed by integrating the continuity equation as we did not have access to the explicit lateral fluxes computed by the models. Specifically, at the northern edge, a no-flux boundary condition was applied and the continuity equation integrated southward starting from the northern boundary. The integration stop at 45° S (about as far south as one can get before it becomes impossible with this approach to separate the Atlantic and Indo-Pacific basins). One concern (raised by a reviewer) with this approach is the northern boundary condition. In many of the models used here there is no Arctic, so a no-flux boundary condition is justified (or at least consistent). CCSM does include the Arctic, but we did not have access to the simulated carbon transports. However, we can estimate its value as follows. Assuming a Bering Strait inflow into the Arctic of ∼1 Sv and an average C_{ant} concentration of 40 µmol kg^{-1} gives a northward transport of ∼0.015 PgC/y. This would shift all the Indo-Pacific curves upward by that amount. The Atlantic curves would shift downward by a similar amount.

In the Atlantic, the largest anthropogenic CO_2 uptake occurs in the Southern Ocean, but much of this uptake is transported equatorward, largely by the northward and downward spreading of Antarctic Intermediate Water (AAIW) and Sub-Antarctic Mode Water (SAMW). Analysis of the basis functions used in Mikaloff Fletcher et al. (2006) suggests that the bulk of this anthropogenic CO_2 is stored in the South Atlantic subtropical gyre. There is also substantial anthropogenic carbon uptake in the tropical Atlantic. While a portion of this tropical uptake is transported southwards, most is either stored in the tropics or transported northwards along the surface before being stored in the subtropical North Atlantic (Mikaloff Fletcher et al., 2006). Anthropogenic CO_2 taken up in the North Atlantic is either transported northwards and entrained into NADW or transported southwards, leading to convergence with the anthropogenic CO_2 being transported northwards from the tropics and Southern Hemisphere at Northern Hemisphere mid-latitudes. While there is overall consistency between different estimates, it should be noted that some of the OIP and EnKF cases have much larger values of uptake, storage and transport in the Southern Ocean and also display a more complex multi-modal latitudinal distribution not seen in the other estimates. The large uptakes in the Southern Ocean are a deficiency of the particular models involved. In the OIP, the model that shows this feature also overestimates CFC uptake in that region compared with observations. (As the reported mean of the OIP is weighted by a skill score based on CFCs, this model does not have much influence on the reported mean result.) In the case of the EnKF, these much larger uptake rates in the Southern Ocean have to do with the too-vigorous convection of the Bern3D model. This vigorous convection was needed to get enough deep water formation, a consequence of the very coarse-resolution of the model in the Southern Ocean.

Transport of anthropogenic CO_2 along ship transects can also be estimated from hydrographic data and data-based anthropogenic CO_2 estimates (e.g., Lundberg and Haugan, 1996; Holfort et al., 1998; Álvarez et al., 2003; Macdonald et al., 2003; Rosón et al., 2003; Álvarez and Gourcuff, 2010). This approach has been widely used in the Atlantic, and a

number of these transect-based estimates have been included in Fig. 6. One crucial difference between transports inferred from the ocean inversion and those inferred from transect data is that the hydrographic transect estimates reflect the transport at a single point in time while the estimates from the ocean inversion represent the time-integrated transport over the entire industrial period, which can then be scaled to a given year. In particular, hydrographic fluxes may be biased due to the neglect of seasonal variability (Wilkin et al., 1995). The transports from the ocean inversion, forward OGCMs, and hydrographic transects have similar large-scale features in the Atlantic, with substantial northward transport occurring throughout the Southern Hemisphere and tropics. The transport across 31° S estimated by Holfort et al. (1998) is substantially smaller than that estimated by the ocean inversion techniques, while that estimated by Holfort et al. (1998) across 20° S is in agreement with this approach. The North Atlantic transport estimates of Rosón et al. (2003) and Macdonald et al. (2003) are larger than those from the ocean inversion, but not unreasonably so given the large uncertainties in the hydrographic estimates and difficulties comparing the two techniques directly. The Indo-Pacific ocean basin follows a similar general pattern to the Atlantic of strong anthropogenic CO_2 uptake at high latitudes, particularly in the Southern Ocean, which is then transported equatorwards to mid-latitudes. Unlike the Atlantic Ocean, however, the Indonesian throughflow (ITF) plays a key role in transports in the tropical and Southern Hemisphere Pacific and Indian oceans (Mikaloff Fletcher et al., 2006). While there is strong northward transport of anthropogenic carbon throughout the Pacific Ocean south of 18° N, as shown for the overall Indo-Pacific basin in Fig. 6, a substantial amount of anthropogenic carbon is transported southwards into the Indian Ocean via the ITF. Note, however, that the maxima in poleward transport in both hemispheres occur at different latitudes in the various estimates, with the GF, ECCO, and CCSM-ETH estimates showing a marked shift toward higher latitudes compared with OIP and EnKF. Anthropogenic carbon taken up in the tropical Indian Ocean or transported via the ITF is transported southwards to mid-latitudes.

3.3 Limitations of the inverse approach

While the large-scale features of the model-based ocean inversion results described above have been shown to be robust (Mikaloff Fletcher et al., 2006; Gerber et al., 2009), there are several sources of error that should be considered in evaluating these results. One major source of uncertainty in the ocean inversion is error in the representation of ocean transport by the OGCM, which is implicitly assumed to be perfect in the inverse methodology. In order to evaluate the sensitivity to the choice of ocean model, Mikaloff Fletcher et al. (2006) used a suite of ten OGCMs to calculate the basis functions. Similarly, Gerber et al. (2009) used four different configurations of a single OGCM to investigate the sensitivity of the inferred fluxes and transport rates to different circulation representations, and arrived at a similar spread between models to that found in Mikaloff Fletcher et al. (2006). This spread is clearly evident in Fig. 6, which shows the flux, storage, and transport from all ten OGCMs used in Mikaloff Fletcher et al.. The largest differences in the inferred air–sea fluxes, storage and transport rates are found in the Southern Ocean, which confirms earlier model studies (Orr et al., 2001). These large differences are attributed to ocean model limitations in the precise formulation of subgrid-scale processes such as eddies and convection, the representation of transport along isopycnals, and brine rejection due to sea ice formation (Mikaloff Fletcher et al., 2006).

There may also be significant biases in the model transport that are common to all of the models and model setups used in both inverse studies discussed here, particularly due to model physical errors (Doney et al., 2004) and the coarse-resolution of the global models used in those studies. Results of forward simulations of transient tracers with eddy-resolving model have recently become available (Lachkar et al., 2009; Ito et al., 2010). The large-scale transport pathways of these models are not completely dissimilar to those of coarse-resolution models. Comparing a transient tracer forward simulation with an eddy-resolving model to a coarse-resolution model, Lachkar et al. (2007) reported a decrease in air–sea flux and inventory of C_{ant} in the Southern Ocean of 23 % and 35 %, respectively. In addition, both inverse studies used OGCMs in steady state and implicitly assumed that the temporal variability was proportional to the atmospheric CO_2 perturbation over the industrial period, which could also lead to biases in the inferred results. There is some evidence for both decadal variability in ocean circulation (e.g., García et al., 2002; Bryden et al., 2003), and there are indications that changes in the oceanic uptake may be responding to climate change (Le Quéré et al., 2007; Lovenduski et al., 2007; Le Quéré et al., 2010).

Another potential source of uncertainty is the method used to reconstruct C_{ant}. Gerber et al. (2009) assimilated four different global and six Atlantic reconstructions of C_{ant} to assess uncertainties from data-based estimates in their inverse approach. Two of the global approaches (ΔC^* and TTD) are shown in Fig. 6 (red lines). The sensitivity of the inferred air–sea fluxes and transport rates to the anthropogenic CO_2 reconstruction method is of similar magnitude to the sensitivity to the choice of OGCM. The deviations in inferred air–sea fluxes and transport rates among the different assimilated reconstructions are largest in the Southern Ocean, which is expected as the largest differences in the anthropogenic carbon storage occur in this region as well (Vázquez-Rodríguez et al., 2009b). The good agreement between inverse estimates using the basis function and EnKF methodologies (Gerber et al., 2009) and between inverse estimates using different region configurations (Mikaloff Fletcher et al., 2006) suggests that the inverse methodology is likely to be only a minor source of uncertainty.

Lastly, we note that the observational estimates of inorganic carbon transport shown in Fig. 6 are also subject to considerable error. These can arise from both uncertainties in the estimated flux of water and the C_{ant} in the water masses involved in the transport (e.g., Schneider et al., 2010). In the North Atlantic, the uncertainty in C_{ant} transport has been estimated to be roughly 0.05–0.08 PgC y^{-1} (Holfort et al. (1998); Rosón et al. (2003); Macdonald et al. (2003); Álvarez et al. (2003); Álvarez and Gourcuff (2010); see Table A4 in the appendix). According to Ganachaud et al. (2000), errors in C_{ant} transport can be reduced significantly when it is computed in term of anomalies from the mean properties.

4 Changes in C_{ant} storage from repeat measurements

4.1 Methods

Thanks to the recent availability of repeat measurements from the global repeat hydrography program, we can now determine not only C_{ant} concentrations using the methods described above but also their rate of change, or the storage rate, on decadal timescales. Measurements of the change in dissolved inorganic carbon or C_{ant} concentration between two time periods may also be less dependent on assumptions made in the methods discussed in the previous section, but might suffer from a different set of potentially biasing assumptions (e.g., Levine et al., 2008; Wanninkhof et al., 2010, see below). Of particular concern is the much larger sensitivity of this approach to changes in the oceans' background distribution of DIC due to variability in ocean currents and biology. These variations largely lead to ocean internal redistributions of "natural" carbon, which needs to be separated from the measured DIC difference in order to extract that part of the changes that is due to the oceans' uptake of anthropogenic CO_2. Multiple Linear Regression (MLR) models or their extended version (eMLR) have been used extensively to filter out this "natural" variability. While many of the estimates presented below (Fig. 7) are based on this approach, there are alternative techniques to calculate the storage rate of C_{ant}. One such method that has been classically applied is to calculate inventories by vertically integrating the C_{ant} concentrations over the entire water column of the area under consideration. If a transient steady state (TSS) (Keeling and Bolin, 1967) is assumed for C_{ant} (Tanhua et al., 2007), the C_{ant} storage rate can be approximated as the product of the time derivative of the average C_{ant} concentration in the winter mixed layer and the mean penetration depth (MPD). The latter is defined as the quotient between the C_{ant} column inventory and the C_{ant} concentration in the winter mixed layer. The studies of Holfort et al. (1998), Rosón et al. (2003), and Álvarez et al. (2003) have applied this approach. The basis for this approximation relies on the fact that MPD may be taken as constant (Broecker, 1979). However, Pérez et al. (2008) have pointed out that the time variability of the MPD could significantly affect estimates of C_{ant} storage rates in, or close to, areas of deep water formation, especially during high NAO periods .

Here, we review published storage estimates of C_{ant} for various regions or hydrographic lines and compare them with estimates made by the Green function approach. The comparison serves to highlight the large temporal variability in CO_2 storage, particularly in Southern Hemisphere mode waters (Murata et al., 2010), that is not captured by back-calculation and other inverse methods. Note that for estimates based on individual sections, storage rates are reported in terms of changes in column inventory (in units of mol $m^{-2}y^{-1}$), while basin-integrated estimates are reported in terms of PgC y^{-1}.

4.2 Results

Atlantic Ocean: Observations from repeat measurements along a north–south section in the Atlantic Ocean suggest that the DIC inventory of the South Atlantic has been increasing at a faster rate than the North Atlantic (Wanninkhof et al., 2010) (left column of Fig. 7). Large variations in the storage rates on subdecadal timescales have been documented in parts of the relatively well sampled subpolar North Atlantic. A significantly smaller increase rate of the C_{ant} inventory than expected from the increase in atmospheric CO_2 has been observed in the western subpolar North Atlantic (Steinfeldt et al., 2009), and storage rates in the Irminger Sea have varied considerably over the last three decades (Pérez et al., 2008). Strong correlation between the North Atlantic Oscillation (NAO) and the C_{ant} storage rate, with a high NAO index corresponding to higher storage, has been demonstrated for the subpolar gyre of the North Atlantic (Pérez et al., 2010), and similar trends are found in the intermediate waters of the subtropical North Atlantic at 24° N (Brown et al., 2010). While estimates of storage rate based on the GF and other inverse approaches are broadly consistent with those derived from hydrographic sections (Fig. 7), there are significant differences as well, likely due in part to the large temporal variability not accounted for by the former. For example, the pattern of higher storage in the South Atlantic relative to the North Atlantic found by Wanninkhof et al. (2010) is not seen in the inverse estimates.

Pacific Ocean: In the Pacific, repeat measurements were made along 13 sections from 2001 up to 2009 (middle column of Fig. 7). In the North Pacific, most of the observed increase in DIC is due to changes in ocean circulation, as indicated by changes in apparent oxygen utilization (AOU), rather than uptake of C_{ant} (Sabine et al., 2008). In contrast, an increase in DIC in the South Pacific can be attributed to uptake of C_{ant} that is absorbed and transported by Southern Ocean-origin water masses such as SAMW and AAIW (Murata et al., 2007). There are significant spatial variations in storage rate across the Pacific basin. For example, both the GF and repeat hydrography estimates show higher storage in

the South compared with the North Pacific (Murata et al., 2007; Sabine et al., 2008). On the other hand, while the GF method and an earlier hydrographic study (Sabine et al., 2008) suggest higher storage rates in the western as compared with the eastern North Pacific, a more recent study (Waters et al., 2011) finds the opposite pattern along 30° S. The latter study is based on data from a section repeated in 1992 and 2010. Note, however, that methods to compute C_{ant} from repeat measurements differ between studies, which could account for some of the reported differences. Note, too, that some observational estimates are not entirely consistent with those based on inverse methods. It is unclear if this reflects real changes in ocean biogeochemistry and ocean circulation that are not captured by inverse methods, or if there are biases in the repeat hydrography-based estimates.

Indian Ocean: Several hydrographic sections in the Indian Ocean were reoccupied between 2002 and 2009, notably the zonal lines I3/I4 and I5 (right column of Fig. 7). Although there are only a few reports of changes in C_{ant} from repeat hydrography in this basin, the trends in the results are generally consistent with the GF approach. The ITF plays an important role in transporting C_{ant} between the Indian and Pacific oceans. This transport is currently not well constrained by observations or global models (Mikaloff Fletcher et al., 2006), but recent repeat measurements along 20° S show influences of ITF on storage rates of C_{ant} (Murata et al., 2010). Results from this study indicate an average storage rate of $1.0\,\mathrm{mol\,m^{-2}\,y^{-1}}$ along 20° S (Fig. 7), with significant increase in C_{ant} to about 1800 m depth, and in the Circumpolar Deep Water. This storage rate is higher than the GF estimate, possibly indicating changes in circulation. A recently published study by Álvarez et al. (2011) indicates that the ventilation of the Subantarctic Water in the subtropical Indian Ocean has increased, potentially enhancing the uptake of C_{ant}.

4.3 Uncertainty

On an ocean basin scale, estimation of C_{ant} storage from repeat measurements also suffers from the issue of sparse sampling discussed earlier. In addition, changes in the natural carbon cycle and circulation may mask or confuse the anthropogenic CO_2 signal. For example, Wanninkhof et al. (2010) found changes in DIC concentration in the Atlantic between 1985 and 2005 that were more varied and larger than could be explained by the uptake of C_{ant} from the atmosphere. Application of the eMLR approach along isopycnals was used to remove variability in the natural carbon cycle. However, as discussed by Wanninkhof et al., (2010) large biogeochemical changes can introduce biases in the eMLR-based estimates. Similarily, Alvarez et al. (2011) found decadal changes in DIC that were smaller than the changes in C_{ant}, which could be explained by enhanced ventilation, i.e., less DIC due to remineralization of organic matter, but more rapid transport of C_{ant} to the interior ocean. The use of MLR methods can potentially compensate for biases due to changing ventilation and circulation when calculating decadal change in C_{ant}. However, the eMLR methods are also sensitive to biases and uncertainty. For instance, a bias in the parameters used for the MLR fit can introduce errors in the estimated change of C_{ant} (e.g., Tanhua et al., 2007). Similarly, Goodkin et al. (2011) found that secular trends from changing climate and changing carbonate chemistry invalidate the use of the MLR technique over time periods larger than about 30 years. We refer to Wanninkhof et al. (2010) for an extensive discussion of estimation of changes in C_{ant} from repeat hydrography. Reported uncertainties (not considering biases in the methodology) of the regional C_{ant} storage rate range between ± 0.01 and $\pm 0.06\,\mathrm{PgC\ y^{-1}}$ or a relative uncertainty between ∼5–25 % (see Table A5 in the appendix).

5 A "best estimate" of the global ocean inventory in 2010

Lastly, we have used the various data- and model-derived estimates to arrive at a "best estimate" of the inventory of anthropogenic CO_2 in the ocean in 2010. As most estimates are for earlier years, we scale them to a nominal year of 2010 by assuming a TSS (e.g., Gammon et al., 1982; Tanhua et al., 2007). This approach essentially states that the concentration (and inventory) of a tracer increases proportionally to its increase in the surface mixed layer, which we can estimate based on the evolution of atmospheric CO_2. The TSS assumes a large-scale ocean circulation and mixing field that is essentially invariant in time, but this assumption has also been made in the determination of all data-based inventories. A compilation of the adjusted estimates are listed in Table 2 for both the region covered by the GLODAP database, i.e., essentially the open ocean without the continental shelf and marginal seas, and the original grid (in the case of models).

The estimates range widely, from 106 PgC to 150 PgC. The mean of the data-based estimates, including those based on ocean inversions, is ≈141 PgC for the GLODAP region, while the corresponding average for the various CCSM model runs is 109 PgC. ECCO, which employs an ocean circulation constrained by observations, gives a larger inventory of 152 PgC. It is important to note that the various data-based estimates are not strictly independent. For example, three of them (ΔC^*, EnkF-ΔC^*, and OIP) depend directly or indirectly on the ΔC^* estimate for 1994, while two of them (TTD and EnKF-TTD) make use of the TTD estimate. The ECCO state estimate – although a different version than that used here – is also a member of the ensemble of models used in OIP. The GF estimate also makes use of information from ECCO in constructing a prior solution, although as discussed previously the incorporation of this information does not lead to results that are much different than from using a model-independent prior. To partially account for this, we first average these interdependent members and then take the mean,

resulting in an inventory of 143 PgC. Given the known biases in both CCSM and ECCO (see Sec. 2.2 and Graven et al. (2012)), we adopt this data-based average as our "best" estimate for the region covered by GLODAP.

To constrain the C_{ant} in marginal seas and continental shelf areas, we exploit results from the CCSM model, which includes the Arctic. The average difference between the inventory for the CCSM global ocean grid and that for the GLODAP region is ∼14 PgC for the year 2010. We regard this as an upper limit on the anthropogenic carbon inventory stored in the excluded region since, as described above, CCSM tends to exhibit low surface-to-deep transport, and hence reduced uptake. This would tend to reduce the inventory in the GLODAP region. On the other hand, uptake in the marginal seas, which are mainly, although not exclusively, shallow shelf areas, is less likely to be biased since CCSM does a reasonable job of simulating upper-ocean C_{ant}. As a lower limit, we use the estimate of Lee et al. (2011), scaled to 2010, of 8.6±0.6 PgC for several marginal basins including the Arctic, the Nordic seas, the Mediterranean Sea, and the East Sea (Sea of Japan) (as discussed in Sec. 2.2, these are computed using either the ΔC^* or TTD methods). This estimate does not cover basins such as the Red Sea, Caribbean, and Gulf of Mexico. We therefore consider it as a lower estimate, leading to a range of ∼9–14 PgC for the region not covered by the GLODAP data set.

Adding the above data-based estimate for the GLODAP region (143 PgC) and the estimated range for the marginal seas (9–14 PgC) gives a range of 152–157 PgC. We adopt the midpoint of this range, 155 PgC, as our "best" estimate for the global ocean inventory of anthropogenic carbon in 2010 with an uncertainty on the order of ±20 %.

6 Summary and conclusions

In this paper, we have reviewed observation-based estimates of the storage and transport of anthropogenic CO_2 in the ocean. We find that considerable progress has been made in efforts to quantify the ocean sink of anthropogenic CO_2. On the global scale, it is reassuring that widely different approaches lead to estimates of the inventory of C_{ant} in the ocean that agree within the uncertainty (typically ∼20 %) of the various methods. Regionally, however, there are significant differences that can be traced to the specific assumptions made by each method. It is also now possible to obtain an estimate of the full time history of the distribution of C_{ant} in the ocean using methods such as Green's functions. An important development is the application of numerical models in an inverse or data-assimilative scheme that allows us to combine data-based estimates of C_{ant} with models to infer the flux, transport, and storage of C_{ant}. These can be difficult to obtain by direct observation. There are caveats in this approach too, notably the sensitivity to model transport and the actual C_{ant} data product used. All of these methods suffer from one important drawback: they suppress or ignore temporal variability and trends. This limitation can be addressed in part by measuring the change in carbon concentration over a period from repeat hydrographic sections to estimate the storage rate of C_{ant}. However, large biogeochemical changes may confuse or mask the C_{ant} signal.

We have also compared anthropogenic C_{ant} simulated by forward ocean biogeochemical models with the data-based estimates. Substantial regional differences exist between forward ocean model C_{ant} fields and data-based estimates, as exhibited by the CCSM model variants that tend to underestimate global C_{ant} inventory. The forward model biases reflect ongoing issues with forward ocean model physical circulation. The data-constrained physical state estimation as exhibited in the ECCO simulation improves the spatial patterns of the simulated C_{ant} field, although some differences with the various data-based estimates remain. This suggests the use of physical state estimates as a weak constraint, such as in the computation of priors required by the Green function approach (with suitable averaging so as to not introduce detailed information about model circulation that is not expected to be accurate (Holzer et al., 2010)). Nevertheless, the experience suggests that forward OGCMs can be improved through careful model–data comparisons and process level studies. Forward OGCMs also offer opportunities to help interpret climate-driven variability and trends, as well as projecting future behavior of ocean carbon storage.

Lastly, a compilation of inventories based on different methods gives us a "best" estimate of about 155 PgC for the global ocean inventory of anthropogenic carbon in 2010. The uncertainty on this estimate is ∼ ±20 %. The large range in various estimates (Table 2), and our comparison of different methods suggests, that multiple approaches, each with its own strengths and weaknesses, remain necessary to quantify the ocean sink of anthropogenic CO_2. Future progress in reducing this uncertainty is likely to come from newer data sets such as GLODAP version 2 and better observational coverage (in both space and time), as well as the development of improved and higher-resolution physical state estimates and combined physical/biogeochemical data assimilation systems that can exploit these data.

Appendix A

The tables in this appendix summarize various published uncertainty estimates discussed in the text.

Table A1. Published estimates of uncertainties in C_{ant} calculation for various estimation methods.

C_{ant} method	C_{ant} concentration uncertainty [$\mu mol\,kg^{-1}$]	Reference	Region
ΔC^*	±9	Gruber et al. (1996)	Global
	±6	Sabine et al. (1999)	Indian Ocean
	±7.5	Sabine et al. (2002)	Pacific Ocean
	±7.9	Lee et al. (2003)	Atlantic Ocean
IPSL	±3 to ±6	Lo Monaco et al. (2005b)	Southern Ocean
Green's function	±2 to ±8	Khatiwala et al. (2009)	Global
TTD	±5	Waugh et al. (2006)	Global
TrOCA	±6.2	Touratier et al. (2007)	Global
ϕC_T^0	±5.2	Vázquez-Rodríguez et al. (2009a,b)	Atlantic Ocean

Table A2. Published estimates of uncertainty in the column inventory of C_{ant}.

C_{ant} method	C_{ant} column inventory uncertainty [$mol\,m^{-2}$]	Reference	Region
ΔC^*	±7.3	Lee et al. (2003)	Atlantic Ocean
	±5.7	Peng et al. (2003)	Pacific Ocean
IPSL	±10	Lo Monaco et al. (2005b)	Southern Ocean
TTD, TrOCA, IPSL, ΔC^*	±2.0 to ±2.3	Álvarez et al. (2009)	Indian Ocean along 30° S
ϕC_T^0	±1 to ±2	Vázquez-Rodríguez et al. (2009a,b)	Atlantic Ocean
Green's function	±10	Khatiwala et al. (2009)	Atlantic Ocean
	±4	Khatiwala et al. (2009)	Pacific Ocean

Table A3. Published estimates of uncertainty in the inventory of C_{ant}. Numbers in bracket indicate the relative uncertainty.

C_{ant} method	C_{ant} inventory uncertainty [PgC] (%)	Reference	Region
ΔC^*	±8.6 (18 %)	Lee et al. (2003)	Atlantic Ocean
ϕC_T^0	±4 (13 %)	Vázquez-Rodríguez et al. (2009a,b)	North Atlantic
ΔC^*	±3 (15 %)	Sabine et al. (1999)	Indian Ocean
ΔC^*	±5 (11 %)	Sabine et al. (2002)	Pacific Ocean
ΔC^*	±17 (16 %)	Sabine et al. (2004)	Global ocean excluding marginal seas
TTD	94–121 (25 %)	Waugh et al. (2006)	Global ocean excluding marginal seas
Green's function	±25 (20 %)	Khatiwala et al. (2009)	Global ocean excluding marginal seas
eMLR	±1 (25 %)	Friis et al. (2005)	Northern North Atlantic
TTD	±0.4 (13 %)	Tanhua et al. (2009)	Arctic Ocean
TTD	±0.4 (24 %)	Schneider et al. (2010)	Mediterranean Sea

Table A4. Published estimates of C_{ant} transport and its uncertainty for different regions.

C_{ant} Region	C_{ant} transport and uncertainty [PgC y^{-1}]	Reference
North Atlantic (24° N)	0.24 ± 0.08	Rosón et al. (2003)
North Atlantic (24° N; 1998)	0.2 ± 0.08	Macdonald et al. (2003)
North Atlantic (24° N; 1992)	0.17 ± 0.06	Macdonald et al. (2003)
North Atlantic (40°–60° N, WOCE A25 section)	0.04 ± 0.05	Álvarez et al. (2003)
North Atlantic (40°–60° N, WOCE A25 section)	0.03 ± 0.015	Álvarez and Gourcuff (2010)
South Atlantic (10°–30° S)	$0.1–0.22 \pm 0.05$	Holfort et al. (1998)

Table A5. Published estimates of C_{ant} storage rate and its uncertainty for different regions.

C_{ant} Region	C_{ant} storage rate and uncertainty [PgC y^{-1}]	Reference
Atlantic (30° S–24° N)	0.17 ± 0.01	Rosón et al. (2003)
North Atlantic (24°-80° N)	0.22 ± 0.06	Macdonald et al. (2003)
North Atlantic (between 24° N and WOCE A25 section)	0.32 ± 0.04	Álvarez et al. (2003)
South Atlantic (10°–30° S)	0.1 ± 0.02	Holfort et al. (1998)

Acknowledgements. We thank Rik Wanninkhof and an anonymous reviewer for their insightful and helpful comments. This work was supported by US NSF grant OCE 10-60804 (Khatiwala); by the New Zealand Foundation for Research Science and Technology with funding support under contract CO1X0703 (Mikaloff-Fletcher); the Spanish project CTM2010-17141 (Ríos); through EU FP7 projects COCOS (Coordinated Action Carbon Observing System) and CARBOCHANGE (changes in carbon uptake and emissions by oceans in a changing climate), which received funding from the European Community's Seventh Framework Programme under grant agreement nos. 212196 and 264879 (Tanhua, Gerber, and Gruber); and by NOAA grant NA07OAR4310098. LDEO contribution no. 7671.

Edited by: J. Canadell

References

Álvarez, M. and Gourcuff, C.: Uncoupled transport of chlorofluorocarbons and anthropogenic carbon in the subpolar North Atlantic, Deep-Sea Res. I, 57, 860–868, doi:10.1016/j.dsr.2010.03.009, 2010.

Álvarez, M., Ríos, A. F., Pérez, F. F., Bryden, H. L., and Rosón, G.: Transports and budgets of total inorganic carbon in the subpolar and temperate North Atlantic, Glob. Biogeochem. Cy., 17 (GB1002), doi:10.1029/2002GB001881, 2003.

Álvarez, M., Lo Monaco, C., Tanhua, T., Yool, A., Oschlies, A., Bullister, J. L., Goyet, C., Metzl, N., Touratier, F., McDonagh, E., and Bryden, H. L.: Estimating the storage of anthropogenic carbon in the subtropical Indian Ocean: a comparison of five different approaches, Biogeosciences, 6, 681–703, doi:10.5194/bg-6-681-2009, 2009.

Álvarez, M., Tanhua, T., Brix, H., Lo Monaco, C., Metzl, N., McDonagh, E., and Bryden, H. L.: Decadal biogeochemical changes in the western Indian Ocean associated with Subantarctic Mode Water, J. Geophys. Res., 116 (C09016), doi:10.1029/2010JC006475, 2011.

Andres, R. J., Boden, T. A., Bréon, F., Ciais, P., Davis, S., Erickson, D., Gregg, J. S., Jacobson, A., Marland, G., Miller, J., Oda, T., Olivier, J. G. J., Raupach, M. R., Rayner, P., and Treanton, K.: A synthesis of carbon dioxide emissions from fossil-fuel combustion, Biogeosciences, 9, 1845–1871, doi:10.5194/bg-9-1845-2012, 2012.

Bousquet, P., Peylin, P., Ciais, P., Le Quéré, C., Friedlingstein, P., and Tans, P. P.: Regional changes in carbon dioxide fluxes of land and oceans since 1980, Science, 290 (5495), 1342–1346, doi:10.1126/science.290.5495.1342, 2000.

Brewer, P. G.: Direct measurements of the oceanic CO_2 increase, Geophys. Res. Lett., 5, 997–1000, 1978.

Broecker, W. S.: "NO" a conservative water mass tracer, Earth and Planet. Sci. Lett., 23, 8761–8776, 1974.

Broecker, W. S.: Revised estimate for the radiocarbon age of North Atlantic Deep Water, J. Geophys. Res., 84, 3218–3226, 1979.

Broecker, W. S., Takahashi, T., and Peng, T.: Reconstruction of past atmospheric CO_2 contents from the chemistry of the contemporary ocean, Tech. Rep. Rep. DOE/OR-857, U.S. Dept. of Energy, Washington, D. C., 1985.

Broecker, W. S., Peacock, S. L., Walker, S., Weiss, R., Fahrbach, E., Schroeder, M., Mikolajewicz, U., Heinze, C., Key, R. M., Peng, T., and Rubin, S.: How much deep water is formed in the Southern Ocean, J. Geophys. Res., 103, 15833–15844, 1998.

Brown, P. J., Bakker, D. C. E., Schuster, U., and Watson, A. J.: Anthropogenic carbon accumulation in the subtropical North Atlantic, J. Geophys. Res., 115 (C04016), doi:10.1029/2008JC005043, 2010.

Bryden, H. L., McDonagh, E. L., and King, B. A.: Changes in ocean water mass properties: Oscillations or trends?, Science, 300, 2086–2088, 2003.

Chen, C.-T. and Millero, F. J.: Gradual increase of oceanic CO_2, Nature, 277, 205–206, 1979.

Denman, K. L., Brasseur, G., Chidthaisong, A., Ciais, P., Cox, P. M., Dickinson, R. E., Hauglustaine, D., Heinze, C., Holland, E., Jacob, D., Lohmann, U., Ramachandran, S., da Silva Dias, P. L., Wofsy, S. C., and Zhang, X.: Couplings Between Changes in the Climate System and Biogeochemistry, in: Climate Change 2007: The Physical Science Basis. Contribution of Working Group I to the Fourth Assessment Report of the Intergovernmental Panel on Climate Change, edited by Solomon, S. and D. Qin and M. Manning and Z. Chen and M. Marquis and K. B. Averyt and M.Tignor and H. L. Miller, Cambridge University Press, Cambridge, UK, 2007.

Doney, S. C., Lindsay, K., Caldeira, K., Campin, J., Drange, H., Dutay, J., Follows, M., Gao, Y., Gnanadesikan, A., Gruber, N., Ishida, A., Joos, F., Madec, G., Maier-Reimer, E., Marshall, J. C., Matear, R. J., Monfray, P., Mouchet, A., Najjar, R., Orr, J. C., Plattner, G., Sarmiento, J., Schlitzer, R., Slater, R., Totterdell, I. J., Weirig, M., Yamanaka, Y., and Yool, A.: Evaluating global ocean carbon models: the importance of realistic physics, Glob. Biogeochem. Cy., 18 (GB3017), doi:10.1029/2003GB002150, 2004.

Doney, S. C., Lima, I., Feely, R. A., Glover, D. M., Lindsay, K., Mahowald, N., Moore, J. K., and Wanninkhof, R.: Mechanisms governing interannual variability in upper-ocean inorganic carbon system and air-sea CO_2 fluxes: Physical climate and atmospheric dust, Deep-Sea Res. II, 56, 640–655, doi:10.1016/j.dsr2.2008.12.006, 2009a.

Doney, S. C., Lima, I., Moore, J. K., Lindsay, K., Behrenfeld, M. J., Westberry, T. K., Mahowald, N., Glover, D. M., and Takahashi, T.: Skill metrics for confronting global upper ocean ecosystem-biogeochemistry models against field and remote sensing data, J. Mar. Sys., 76, 95–112, doi:10.1016/j.jmarsys.2008.05.015, 2009b.

Enting, I. G. and Mansbridge, J. V.: Seasonal Sources and Sinks of Atmospheric CO_2: Direct Inversion of Filtered Data., Tellus B, 41, 11–126, 1989.

Evensen, G.: The Ensemble Kalman Filter: theoretical formulation and practical implementation, Ocean Dynam., 53, 343–367, 2003.

Friis, K.: A review of marine anthropogenic CO_2 definitions: introducing a thermodynamic approach based on observations, Tellus, 58B, 2–15, doi:10.1111/j.1600-0889.2005.00173.x, 2006.

Friis, K., Körtzinger, A., Pätsch, J., and Wallace, D. W. R.: On the temporal increase of anthropogenic CO_2 in the subpolar North Atlantic, Deep-Sea Res. I, 52, 681–698, doi:10.1016/j.dsr.2004.11.017, 2005.

Fung, I., Doney, S. C., Lindsay, K., and John, J.: Evolution of carbon sinks in a changing climate, Proc. Natl. Acad. Sci., 102, 11201–11206, 2005.

Gammon, R. H., Cline, J., and Wisegarver, D. P.: Chluorofluoromethanes in the northeast Pacific Ocean: Measured vertical distribution and application as transient tracers of upper ocean mixing, J. Geophys. Res., 87, 9441–9454, 1982.

Ganachaud, A., Wunsch, C., Marotzke, J., and Toole, J.: Meridional overturning and large-scale circulation of the Indian Ocean, J. Geophys. Res., 105, 26117–26134, 2000.

García, M. A., Bladé, I., Cruzado, A., Velásquez, Z., García, H., Puigdefabregas, J., and Sospedra, J.: Observed variability of water properties and transports on the World Ocean Circulation Experiment SR1b section across the Antarctic Circumpolar Current, J. Geophys. Res., 107, doi:10.1029/2000JC000277, 2002.

Gerber, M. and Joos, F.: Carbon sources and sinks from an Ensemble Kalman Filter ocean data assimilation, Glob. Biogeochem. Cy., 24, GB3004, doi:10.1029/2009GB003531, 2010.

Gerber, M., Joos, F., Vázquez Rodríguez, M., Touratier, F., and Goyet, C.: Regional air-sea fluxes of anthropogenic carbon inferred with an Ensemble Kalman Filter, Glob. Biogeochem. Cy., 23, GB1013, doi:10.1029/2008GB003247, 2009.

Gloor, M., Gruber, N., Hughes, T. M. C., and Sarmiento, J. L.: An inverse modeling method for estimation of net air-sea fluxes from bulk data: Methodology and application to the heat cycle, Glob. Biogeochem. Cy., 15, 767–782, 2001.

Gloor, M., Gruber, N., Sarmiento, J. L., Sabine, C. L., Feely, R. A., and Rödenbeck, C.: A first estimate of present and preindustrial air-sea CO_2 flux patterns based on ocean interior carbon measurements and models, Geophys. Res. Lett., 30, 1010, 767–782, doi:10.1029/2002GL015594, 2003.

Goodkin, N. F., Levine, N., Doney, S. C., and Wanninkhof, R.: Impacts of temporal CO_2 and climate trends on the detection of ocean anthropogenic CO_2 accumulation, Glob. Biogeochem. Cy., 25, GB3023, doi:10.1029/2010GB004009, 2011.

Graven, H. D., Gruber, N., Key, R., Khatiwala, S., and Giraud, X.: Changing controls on oceanic radiocarbon: New insights on shallow-to-deep ocean exchange and anthropogenic CO_2 uptake, J. Geophys. Res., 117, doi:10.1029/2012JC008074, 2012.

Gruber, N.: Anthropogenic CO_2 in the Atlantic Ocean, Glob. Biogeochem. Cy., 12, 165–191, 1998.

Gruber, N., Sarmiento, J. L., and Stocker, T. F.: An improved method for detecting anthropogenic CO_2 in the oceans, Glob. Biogeochem. Cy., 10, 809–837, 1996.

Gruber, N., Gloor, M., Fan, S., and Sarmiento, J. L.: Air-sea flux of oxygen estimated from bulk data: Implications for the marine and atmospheric oxygen cycles, Glob. Biogeochem. Cy., 15 (4), 783–804, 2001.

Gruber, N., Gloor, M., Mikaloff Fletcher, S. E., Doney, S. C., Dutkiewicz, S., Follows, M. J., Gerber, M., Jacobson, A. R., Joos, F., Lindsay, K., Menemenlis, D., Mouchet, A., Müller, S. A., Sarmiento, J. L., and Takahashi, T.: Oceanic sources, sinks, and transport of atmospheric CO_2, Glob. Biogeochem. Cy., 23, GB1005, doi:10.1029/2008GB003349, 2009.

Hall, T. M., Haine, T. W. N., and Waugh, D. W.: Inferring the concentration of anthropogenic carbon in the ocean from tracers, Glob. Biogeochem. Cy., 16 (GB1131), doi:10.1029/2001GB001835, 2002.

Hall, T. M., Waugh, D. W., Haine, T. W. N., Robbins, P. E., and Khatiwala, S.: Estimates of anthropogenic carbon in the Indian Ocean with allowance for mixing and time-varying air-sea CO_2 disequilibrium, Glob. Biogeochem. Cy., 18, GB1031, doi:10.1029/2003GB002120, 2004.

Holfort, J., Johnson, K. M., Putzka, A., Schneider, B., Siedler, G., and Wallace, D. W. R.: The meridional transport of inorganic carbon in the South Atlantic Ocean, Glob. Biogeochem. Cy., 12, 479–499, 1998.

Holzer, M. and Hall, T. M.: Transit-time and tracer-age distributions in geophysical flows, J. Atmos. Sci., 57, 3539–3558, 2000.

Holzer, M., Primeau, F., Smethie, W., and Khatiwala, S.: Where and how long ago was water in the western North Atlantic ventilated? Maximum-entropy inversions of bottle data from WOCE line A20, J. Geophys. Res., 115 C07005, doi:10.1029/2009JC005750, 2010.

Houghton, R. A., Hackler, J. L., and Lawrence, K. T.: The U.S. carbon budget: Contributions from land-use change, Science, 285, 5427, 574–578, doi:10.1126/science.285.5427.574, 1999.

Ito, T., Woloszyn, M., and Mazloff, M.: Anthropogenic carbon dioxide transport in the Southern Ocean driven by Ekman flow, Nature, 463, 80–83, 10.1038/nature08687, 2010.

Keeling, C. D. and Bolin, B.: The simultaneous use of chemical tracers in oceanic studies, Tellus, 19, 566–581, 1967.

Key, R. M., Kozyr, A., Sabine, C., Lee, K., Wanninkhof, R., Bullister, J., Feely, R. A., Millero, F., Mordy, C., and Peng, T.-H.: A global ocean carbon climatology: Results from GLODAP, Glob. Biogeochem. Cy., 18, GB4031, doi:10.1029/2004GB002247, 2004.

Khatiwala, S.: A computational framework for simulation of biogeochemical tracers in the ocean, Glob. Biogeochem. Cy., 21, GB3001, doi:10.1029/2007GB002923, 2007.

Khatiwala, S.: Fast spin up of ocean biogeochemical models using matrix-free Newton-Krylov, Ocean Modell., 23, 121–129, doi:10.1016/j.ocemod.2008.05.002, 2008.

Khatiwala, S., Visbeck, M., and Schlosser, P.: Age tracers in an ocean GCM, Deep-Sea Res. I, 48, 1423–1441, 2001.

Khatiwala, S., Primeau, F., and Hall, T.: Reconstruction of the history of anthropogenic CO_2 concentrations in the ocean, Nature, 462, 346–349, doi:10.1038/nature08526, 2009.

Körtzinger, A., Mintrop, L., and Duinker, J. C.: On the penetration of anthropogenic CO_2 into the North Atlantic Ocean, J. Geophys. Res., 103, 18681–18689, 1998.

Lachkar, Z., Orr, J. C., Dutay, J.-C., and Delecluse, P.: Effects of mesoscale eddies on global ocean distributions of CFC-11, CO_2, and $\Delta^{14}C$, Ocean Sci., 3, 461–482, doi:10.5194/os-3-461-2007, 2007.

Lachkar, Z., Orr, J. C., and Dutay, J.-C.: Seasonal and mesoscale variability of oceanic transport of anthropogenic CO_2, Biogeosciences, 6, 2509–2523, doi:10.5194/bg-6-2509-2009, 2009.

Large, W. and Yeager, S.: Diurnal to decadal global forcing for ocean and sea-ice models: the datasets and flux climatologies, Tech. Rep. NCAR Technical Note: NCAR/TN-460+STR, CGD Division of the National Centre for Atmospheric Research, Boulder, CO, USA, 2004.

Le Quéré, C., Rödenbeck, C., Buitenhuis, E. T., Conway, T. J., Langenfelds, R., Gomez, A., Labuschagne, C., Ramonet, M., Nakazawa, T., Metzl, N., Gillett, N., and Heimann, M.: Saturation of the Southern Ocean CO_2 sink due to recent climate change, Science, 316, 1735–1738, doi:10.1126/science.1136188, 2007.

Le Quéré, C., Takahashi, T., Buitenhuis, E. T., Rödenbeck, C., and Sutherland, S. C.: Impact of climate change and variability on

the global oceanic sink of CO_2, Glob. Biogeochem. Cy., 24, GB4007, doi:10.1029/2009GB003599, 2010.

Lee, K., Choi, S., Park, G., Wanninkhof, R., Peng, T. H., Key, R. M., Sabine, C. L., Feely, R. A., Bullister, J. L., Millero, F. J., and Kozyr, A.: An updated anthropogenic CO_2 inventory in the Atlantic Ocean, Glob. Biogeochem. Cy., 17, GB1116, doi:10.1029/2003GB002067, 2003.

Lee, K., Sabine, C. L., Tanhua, T., Kim, T. W., Feely, R. A., and Kim, H. C.: Roles of marginal seas in absorbing and storing fossil fuel CO_2, Energy Environ. Sci., 4, 1133–1146, doi:10.1029/2003GB002067, 2011.

Levine, N. M., Doney, S. C., Wanninkhof, R., Lindsay, K., and Fung, I. Y.: Impact of ocean carbon system variability on the detection of temporal increases in anthropogenic CO_2, J. Geophys. Res., 113, C03019, doi:10.1029/2007JC004153, 2008.

Levine, N. M., Doney, S. C., Lima, I., Wanninkhof, R., Bates, N. R., and Feely, R. A.: The impact of the North Atlantic Oscillation on the uptake and accumulation of anthropogenic CO_2 by North Atlantic Ocean mode waters, Glob. Biogeochem. Cy., 25, GB3022, doi:10.1029/2010GB003892, 2011.

Lo Monaco, C., Goyet, C., Metzl, N., Poisson, A., and Touratier, F.: Distribution and inventory of anthropogenic CO_2 in the Southern Ocean: Comparison of three data-based methods, J. Geophys. Res., 110, C09S02, doi:10.1029/2004JC002571, 2005a.

Lo Monaco, C., Metzl, N., Poisson, A., Brunet, C., and Schauer, B.: Anthropogenic CO_2 in the Southern Ocean: Distribution and inventory at the Indian-Atlantic boundary (World Ocean Circulation Experiment line I6), J. Geophys. Res., 110, C06010, doi:10.1029/2004JC002643, 2005b.

Long, M. C., Lindsay, K., Peacock, S., Moore, J. K., and Doney, S. C.: 20th Century ocean carbon uptake and storage in CESM1-BGC, J. Climate, in press, 2012.

Lovenduski, N. S., Gruber, N., Doney, S. C., and Lima, I. D.: Enhanced CO_2 outgassing in the Southern Ocean from a positive phase of the Southern Annular Mode, Glob. Biogeochem. Cy., 21, GB2026, doi:10.1029/2006GB002900, 2007.

Lundberg, L. and Haugan, P. M.: A Nordic Seas Arctic Ocean carbon budget from volume flows and inorganic carbon data, Glob. Biogeochem. Cy., 10, 493–510, 1996.

Macdonald, A. M., Baringer, M. O., Wanninkhof, R., Lee, K., and Wallace, D. W. R.: A 1998–1992 comparison of inorganic carbon and its transport across 24.5° N in the Atlantic, Deep-Sea Res. II, 50, 3041–3064, doi:10.1016/j.dsr2.2003.07.009, 2003.

Marshall, J., Adcroft, A., Hill, C., Perelman, L., and Heisey, C.: A finite-volume, incompressible Navier-Stokes model for studies of the ocean on parallel computers, J. Geophys. Res., 102, 5733–5752, 1997.

Matear, R. J. and McNeil, B. I.: Decadal accumulation of anthropogenic CO_2 in the Southern Ocean: A comparison of CFC-age derived estimates to multiple-linear regression estimates, Glob. Biogeochem. Cy., 17, GB1113, doi:10.1029/2003GB002089, 2003.

Matsumoto, K. and Gruber, N.: How accurate is the estimation of anthropogenic carbon in the ocean? An evaluation of the ΔC^* method, Glob. Biogeochem. Cy., 19, GB3014, doi:10.1029/2004GB002397, 2005.

McKinley, G. A., Fay, A. R., Takahashi, T., and Metzl, N.: Convergence of atmospheric and North Atlantic carbon dioxide trends on multidecadal timescales, Nature Geosci., 4, 606–610, doi:10.1038/NGEO1193, 2011.

Mikaloff Fletcher, S. E., Gruber, N., Jacobson, A. R., Doney, S. C., Dutkiewicz, S., Gerber, M., Follows, M., Joos, F., Lindsay, K., Menemenlis, D., Mouchet, A., Mu uller, S. A., , and Sarmiento, J. L.: Inverse estimates of anthropogenic CO_2 uptake, transport, and storage by the ocean, Glob. Biogeochem. Cy., 20, GB2002, doi:10.1029/2005GB002530, 2006.

Mikaloff Fletcher, S. E., Gruber, N., Jacobson, A. R., Gloor, M., Doney, S. C., Dutkiewicz, S., Gerber, M., Follows, M., Joos, F., Lindsay, K., Menemenlis, D., Mouchet, A., Müller, S. A., and Sarmiento, J. L.: Inverse estimate of the oceanic sources and sinks of natural CO_2 and the implied oceanic carbon transport, Glob. Biogeochem. Cy., 21, GB1010, doi:10.1029/2006GB002751, 2007.

Murata, A., Kumamoto, Y., Watanabe, S., and Fukasawa, M.: Decadal increases of anthropogenic CO_2 in the South Pacific subtropical ocean along 32°S, J. Geophys. Res., 112, C05033, doi:10.1029/2005JC003405, 2007.

Murata, A., Kumamoto, Y., Sasaki, K., Watanabe, S., and Fukasawa, M.: Decadal increases of anthropogenic CO_2 in the subtropical South Atlantic Ocean along 30° S, J. Geophys. Res., 113, C06007, doi:10.1029/2007JC004424, 2008.

Murata, A., Kumamoto, Y., Sasaki, K., Watanabe, S., and Fukasawa, M.: Decadal increases of anthropogenic CO_2 along 149° E in the western North Pacific, J. Geophys. Res., 114, C04018, doi:10.1029/2008JC004920, 2009.

Murata, A., Kumamoto, Y., Sasaki, K., Watanabe, S., and Fukasawa, M.: Decadal increases in anthropogenic CO_2 along 20° S in the South Indian Ocean, J. Geophys. Res., 115, C12055, doi:10.1029/2010JC006250, 2010.

Olsen, A., Omar, A. M., Bellerby, R. G. J., Johannessen, T., Ninnemann, U., Brown, K. R., Olsson, K. A., Olafsson, J., Nondal, G., Kivimae, C., Kringstad, S., Neill, C., and Olafsdottir, S.: Magnitude and origin of the anthropogenic CO_2 increase and ^{13}C Suess effect in the Nordic seas since 1981, Glob. Biogeochem. Cy., 20, GB3027, doi:10.1029/2005GB002669, 2006.

Olsen, A., Omar, A. M., Jeansson, E., Anderson, L. G., and Bellerby, R. G. J.: Nordic seas transit time distributions and anthropogenic CO_2, J. Geophys. Res., 115, C05005, doi:10.1029/2009JC005488, 2010.

Orr, J. C., Najjar, R., Sabine, C. L., and Joos, F.: Abiotic-HOWTO, in: Internal OCMIP Report (www.ipsl.jussieu.fr/OCMIP), 15 pp., LSCE/CEA Saclay, Gif-sur-Yvette, France, 1999.

Orr, J. C., Maier-Reimer, E., Mikolajewicz, U., Monfray, P., Sarmiento, J. L., Toggweiler, J. R., Taylor, N. K., Palmer, J., Gruber, N., Sabine, C. L., Le Quéré, C., Key, R. M., and Boutin, J.: Estimates of anthropogenic carbon uptake from four three-dimensional global ocean models, Glob. Biogeochem. Cy., 15, 43–60, 2001.

Orr, J. C., Fabry, V. J., Aumont, O., Bopp, L., Doney, S. C., Feely, R. A., Gnanadesikan, A., Gruber, N., Ishida, A., Joos, F., Key, R. M., Lindsay, K., Maier-Reimer, E., Matear, R., Monfray, P., Mouchet, A., Najjar, R. G., Plattner, G., Rodgers, K. B., Sabine, C. L., Sarmiento, J. L., Schlitzer, R., Slater, R. D., Totterdell, I. J., Weirig, M., Yamanaka, Y., and Yool, A.: Anthropogenic ocean acidification over the twenty-first century and its impact on marine calcifying organisms, Nature, 437, 681–686, 2005.

Pardo, P. C., Vázquez-Rodríguez, M., Pérez, F. F., and Ríos, A. F.: CO_2 air-sea disequilibrium and preformed alkalinity in

the Pacific and Indian oceans calculated from subsurface layer data, J. Mar. Sys., 84, 67–77, doi:10.1016/j.jmarsys.2010.08.006, 2011.

Park, G., Lee, K., Tishchenko, P., Min, D., Warner, M. J., Talley, L. D., Kang, D., and Kim, K.: Large accumulation of anthropogenic CO_2 in the East (Japan) Sea and its significant impact on carbonate chemistry, Glob. Biogeochem. Cy., 20, GB4013, doi:10.1029/2005GB002676, 2006.

Peng, T., Wanninkhof, R., Bullister, J. L., Feely, R. A., and Takahashi, T.: Quantification of decadal anthropogenic CO_2 uptake in the ocean based on dissolved inorganic carbon measurements, Nature, 396, 560–563, 1998.

Peng, T., Wanninkhof, R., and Feely, R. A.: Increase of anthropogenic CO_2 in the Pacific Ocean over the last two decades, Deep-Sea Res., 50, 3065–3082, 2003.

Pérez, F. F., Vázquez-Rodríguez, M., Louarn, E., Padín, X. A., Mercier, H., and Ríos, A. F.: Temporal variability of the anthropogenic CO_2 storage in the Irminger Sea, Biogeosciences, 5, 1669–1679, doi:10.5194/bg-5-1669-2008, 2008.

Pérez, F. F., Vázquez-Rodríguez, M., Mercier, H., Velo, A., Lherminier, P., and Ríos, A. F.: Trends of anthropogenic CO_2 storage in North Atlantic water masses, Biogeosciences, 7, 1789–1807, doi:10.5194/bg-7-1789-2010, 2010.

Ríos, A. F., Fraga, F., and Pérez, F. F.: Estimation of coefficients for the calculation of "NO", "PO" and "CO", starting from the elemental composition of natural phytoplankton, Sci. Mar., 53, 779–784, 1989.

Ríos, A. F., Álvarez-Salgado, X. A., Pérez, F. F., Bingler, L. S., Arístegui, J., and Mémery, L.: Carbon dioxide along WOCE line A14: Water masses characterization and anthropogenic entry, J. Geophys. Res., 108 (3123), 3065–3082, doi:10.1029/2000JC000366, 2003.

Ríos, A. F., Velo, A., Pardo, P. C., Hoppema, M., and Pérez, F. F.: An update of anthropogenic CO_2 storage rates in the western South Atlantic basin and the role of Antarctic Bottom Water, J. Mar. Syst., 94, 197–203, doi:10.1016/j.jmarsys.2011.11.023, 2012.

Rosón, G., Ríos, A. F., Pérez, F. F., Lavin, A., and Bryden, H. L.: Carbon distribution, fluxes and budgets in the subtropical North Atlantic Ocean (24.5° N), J. Geophys. Res., 108 (C5), doi:10.1029/1999JC000047, 2003.

Roy, T., Bopp, L., Gehlen, M., Schneider, B., Cadule, P., Frölicher, T. L., Segschneider, J., Tjiputra, J., Heinze, C., and Joos, F.: Regional impacts of climate change and atmospheric CO_2 on future ocean carbon uptake: A multi-model linear feedback analysis, J. Climate, 24, 2300–2318, 2011.

Sabine, C. L. and Tanhua, T.: Estimation of anthropogenic CO_2 inventories in the Ocean, Annu. Rev. of Mar. Sci., 2, 175–198, doi:10.1146/annurev-marine-120308-080947, 2010.

Sabine, C. L., Key, R. M., Johnson, K. M., Millero, F. J., Poisson, A., Sarmiento, J. L., Wallace, D. W. R., and Winn, C. D.: Anthropogenic CO_2 inventory of the Indian Ocean, Glob. Biogeochem. Cy., 13, 179–198, 1999.

Sabine, C. L., Feely, R. A., Key, R. M., Bullister, J. L., Millero, F. J., Lee, K., Peng, T. H., Tilbrook, B., Ono, T., and Wong, C. S.: Distribution of anthropogenic CO_2 in the Pacific Ocean, Glob. Biogeochem. Cy., 16, GB1083, doi:10.1029/2001GB001639, 2002.

Sabine, C. L., Feely, R. A., Gruber, N., Key, R. M., Lee, K., Bullister, J. L., Wanninkhof, R., Wong, C. S., Wallace, D. W. R., Tilbrook, B., Millero, F. J., Peng, T., Kozyr, A., Ono, T., and Rios, A. F.: The Ocean Sink for Anthropogenic CO_2, Science, 305, 367–371, 2004.

Sabine, C. L., Feely, R. A., Millero, F., Dickson, A. G., Langdon, C., Mecking, S., and Greeley, D.: Decadal changes in Pacific Carbon, J. Geophys. Res., 113, C07021, doi:10.1029/2007JC004577, 2008.

Sarmiento, J. L., Orr, J. C., and Siegenthaler, U.: A perturbation simulation of CO_2 uptake in an ocean general circulation model, J. Geophys. Res., 97, 3621–3645, 1992.

Schneider, A., Tanhua, T., Körtzinger, A., and Wallace, D. W. R.: High anthropogenic carbon content in the eastern Mediterranean, J. Geophys. Res., 115, C12050, doi:10.1029/2010JC006171, 2010.

Seshadri, V.: The Inverse Gaussian Distribution, Springer, New York, 1999.

Stammer, D., Ueyoshi, K., Köhl, A., Large, W. G., Josey, S. A., and Wunsch, C.: Estimating air-sea fluxes of heat, freshwater, and momentum through global ocean data assimilation, J. Geophys. Res., 109, C05023, doi:10.1029/2003JC002082, 2004.

Steinfeldt, R., Rhein, M., Bullister, J. L., and Tanhua, T.: Inventory changes in anthropogenic carbon from 1997-2003 in the Atlantic Ocean between 20°S and 65° N, Glob. Biogeochem. Cy., 23, GB3010, doi:10.1029/2008GB003311, 2009.

Sweeney, C., Gloor, E., Jacobson, A. R., Key, R. M., McKinley, G., Sarmiento, J. L., and Wanninkhof, R.: Constraining global air-sea gas exchange for CO_2 with recent bomb ^{14}C measurements, Glob. Biogeochem. Cy., 21, GB2015, doi:10.1029/2006GB002784, 2007.

Takahashi, T., Sutherland, S. C., Sweeney, C., Poisson, A., Metzl, N., Tillbrook, B., Bates, N., Wanninkhof, R., Feely, R. A., Sabine, C., Olafsson, J., and Nojiri, Y.: Global sea-air CO_2 flux based on climatological surface ocean pCO2, and seasonal biological and temperature effects, Deep-Sea Res. II, 49, 1601–1622, 2002.

Tanhua, T., Körtzinger, A., Friis, K., Waugh, D. W., and Wallace, D. W. R.: Pacific Ocean heat transport at 24° N in a high resolution global model, Proc. Natl. Acad. Sci., 104, 3037–3042, 2007.

Tanhua, T., Waugh, D. W., and Wallace, D. W. R.: Use of SF_6 to estimate anthropogenic CO_2 in the upper ocean, J. Geophys. Res., 113, C04037, doi:10.1029/2007JC004416, 2008.

Tanhua, T., Jones, E. P., Jeansson, E., Jutterström, S., Smethie Jr., W. M., Wallace, D. W. R., and Anderson, L. G.: Ventilation of the Arctic Ocean: Mean ages and inventories of anthropogenic CO_2 and CFC-11, J. Geophys. Res., 114, C01002, doi:10.1029/2008JC004868, 2009.

Tans, P. P., Fung, I. Y., and Takahashi, T.: Observational contraints on the global atmospheric CO_2 budget, Science, 247, 1431–1439, doi:10.1126/science.247.4949.1431, 1990.

Tarantola, A.: Inverse Problem Theory and Methods for Model Parameter Estimation, SIAM, Philadelphia, PA, USA, 2005.

Touratier, F. and Goyet, C.: Definition, properties, and Atlantic Ocean distribution of the new tracer TrOCA, J. Mar. Sys., 46, 169–179, 2004.

Touratier, F., Azouzi, L., and Goyet, C.: CFC-11, $\Delta^{14}C$ and ^3H tracers as a means to assess anthropogenic CO_2 concentrations in the ocean, Tellus, 59, 318–325, 2007.

Vázquez-Rodríguez, M., Padin, X. A., Ríos, A. F., Bellerby, R. G. J., and Pérez, F. F.: An upgraded carbon-based method to estimate the anthropogenic fraction of dissolved CO_2 in

the Atlantic Ocean, Biogeosciences Discuss., 6, 4527–4571, doi:10.5194/bgd-6-4527-2009, 2009a.

Vázquez-Rodríguez, M., Touratier, F., Lo Monaco, C., Waugh, D. W., Padin, X. A., Bellerby, R. G. J., Goyet, C., Metzl, N., Ríos, A. F., and Pérez, F. F.: Anthropogenic carbon distributions in the Atlantic Ocean: data-based estimates from the Arctic to the Antarctic, Biogeosciences, 6, 439–451, doi:10.5194/bg-6-439-2009, 2009b.

Vázquez-Rodríguez, M., Padín, X. A., Ríos, A. F., and Pérez, F. F.: The subsurface layer memory of water mass formation conditions in the Atlantic: A reliable reference to estimate preformed properties and air-sea CO_2 disequilibria, J. Mar. Sys., 92, 52–63, doi:10.1016/j.jmarsys.2011.10.008, 2012.

Wakita, M., Watanabe, S., Murata, A., Tsurushima, N., and Honda, M.: Decadal change of dissolved inorganic carbon in the subarctic western North Pacific Ocean, Tellus B, 62, 608–620, 2010.

Wang, S., Moore, J. K., Primeau, F., and Khatiwala, S.: Simulation of anthropogenic CO_2 uptake in the CCSM3.1 ocean circulation-biogeochemical model: comparison with data-based estimates, Biogeosciences, 9, 1321–1336, doi:10.5194/bg-9-1321-2012, 2012.

Wanninkhof, R.: Relationship between wind speed and gas exchange over the ocean, J. Geophys. Res., 97, 7373–7382, 1992.

Wanninkhof, R., Doney, S. C., Bullister, J. L., Levine, N. M., Warner, M., and Gruber, N.: Detecting anthropogenic CO_2 changes in the interior Atlantic Ocean between 1989 and 2005, J. Geophys. Res., 115, C11028, doi:10.1029/2010JC006251, 2010.

Waters, J. F., Millero, F. J., and Sabine, C. L.: Changes in South Pacific anthropogenic carbon, Glob. Biogeochem. Cy., 25, GB4011, doi:10.1029/2010GB003988, 2011.

Waugh, D. W., Haine, T. W., and Hall, T. M.: Transport times and anthropogenic carbon in the subpolar North Atlantic Ocean, Deep Sea Res. I, 51, 1475–1491, 2004.

Waugh, D. W., Hall, T. M., McNeil, B. I., Key, R. M., and Matear, R. J.: Anthropogenic CO_2 in the oceans estimated using transit-time distributions, Tellus B, 58, 376–390, 2006.

Wetzel, P., Winguth, A., and Maier-Reimer, E.: Sea-to-air CO_2 flux from 1948 to 2003: A model study, Glob. Biogeochem. Cy., 19, GB2005, doi:10.1029/2004GB002339, 2005.

Wilkin, J. L., Mansbridge, J. V., and Godfrey, J. S.: Pacific Ocean heat transport at 24° N in a high resolution global model, J. Phys. Oceanogr., 25, 2204–2214, 1995.

Wunsch, C. and Heimbach, P.: Practical global oceanic state estimation, Physica D, 230, 197–208, 2007.

Yeager, S. G., Shields, C. A., Large, W. G., and Hack, J. J.: The low-resolution CCSM3, J. Clim., 19, 2545–2566, 2006.

Yool, A., Oschlies, A., Nurser, A. J. G., and Gruber, N.: A model-based assessment of the TrOCA approach for estimating anthropogenic carbon in the ocean, Biogeosciences, 7, 723–751, doi:10.5194/bg-7-723-2010, 2010.